

# Optimized unrestricted Kohn–Sham potentials from *ab initio* spin densities

Katharina Boguslawski,<sup>1</sup> Christoph R. Jacob,<sup>2,a)</sup> and Markus Reiher<sup>1,a)</sup>

<sup>1</sup>ETH Zurich, Laboratorium für Physikalische Chemie, Wolfgang-Pauli-Str. 10, CH-8093 Zurich, Switzerland

<sup>2</sup>Karlsruhe Institute of Technology (KIT), Center for Functional Nanostructures, Wolfgang-Gaede-Straße 1a, 76131 Karlsruhe, Germany

(Received 20 November 2012; accepted 8 January 2013; published online 29 January 2013)

The reconstruction of the exchange–correlation potential from accurate *ab initio* electron densities can provide insights into the limitations of the currently available approximate functionals and provide guidance for devising improved approximations for density-functional theory (DFT). For open-shell systems, the spin density is introduced as an additional fundamental variable in spin-DFT. Here, we consider the reconstruction of the corresponding unrestricted Kohn–Sham (KS) potentials from accurate *ab initio* spin densities. In particular, we investigate whether it is possible to reconstruct the spin exchange–correlation potential, which determines the spin density in unrestricted KS-DFT, despite the numerical difficulties inherent to the optimization of potentials with finite orbital basis sets. We find that the recently developed scheme for unambiguously singling out an optimal optimized potential [Ch. R. Jacob, *J. Chem. Phys.* **135**, 244102 (2011)] can provide such spin potentials accurately. This is demonstrated for two test cases, the lithium atom and the dioxygen molecule, and target (spin) densities from full configuration interaction and complete active space self-consistent field calculations, respectively. © 2013 American Institute of Physics. [<http://dx.doi.org/10.1063/1.4788913>]

## I. INTRODUCTION

Density-functional theory (DFT) within the Kohn–Sham (KS) framework<sup>1,2</sup> represents one of the most frequently applied quantum-chemical methods for electronic structure calculations and for the determination of molecular properties. Its success relies on the accuracy of existing approximations to the exchange–correlation (xc) energy functional  $E_{xc}[\rho]$  and to the xc potential  $v_{xc}[\rho] = \delta E_{xc}[\rho]/\delta\rho$ , i.e., the functional derivative of  $E_{xc}[\rho]$  with respect to the electron density  $\rho(\mathbf{r})$ .<sup>3</sup> However, for open-shell systems, in particular for transition metal complexes, the existing approximations have a number of severe shortcomings,<sup>4–6</sup> for instance, for the prediction of the energy differences between different spin states<sup>7–11</sup> and of spin-density distributions.<sup>12–15</sup>

While the universal functionals  $E_{xc}[\rho]$  and  $v_{xc}[\rho]$  are unknown, there exists a numerical recipe for obtaining the exact xc potential  $v_{xc}[\rho_0]$  corresponding to the ground-state electron density  $\rho_0$  of arbitrary atomic and molecular systems. First, this ground-state electron density  $\rho_0$  can be calculated accurately—and in principle exactly—using wave-function based *ab initio* calculations. Second, the Kohn–Sham potential  $v_s[\rho_0]$  that yields the density  $\rho_0$  in a noninteracting system can be reconstructed. Finally, by subtracting the known nuclear and Coulomb potentials from this reconstructed potential, the xc potential  $v_{xc}[\rho_0]$  can be obtained. Such reconstructed ground-state xc potentials can provide guidance for the construction of approximate xc potentials<sup>16–19</sup> and energy functionals.<sup>20–22</sup>

The key step in the above recipe is the reconstruction of the potential  $v_s[\rho_0]$  from the target density  $\rho_0$ . This step

corresponds to an inverse problem in quantum chemistry,<sup>23</sup> i.e., the potential is sought which generates a given target density in a noninteracting reference system. This potential reconstruction is also essential for quantum-chemical subsystem and embedding methods (for a review, see Ref. 24), in which it can be used to avoid the need for approximating the nonadditive kinetic-energy,<sup>25–30,32</sup> or for developing better approximations for this part of the embedding potential.<sup>31–33</sup>

The inverse problem of reconstructing the noninteracting local potential yielding a given target density is equivalent to evaluating the functional derivative of the noninteracting kinetic-energy functional  $T_s[\rho]$ ,<sup>34,35</sup> which is an implicit functional of the electron density. For evaluating such functional derivatives of implicit functionals, the optimized effective potential (OEP) method can be employed, which tackles the inverse problem by minimizing the implicit functional with respect to the local potential,<sup>36–38</sup> possibly subjected to additional constraints.<sup>39</sup> Thus, the reconstruction of local potentials is a special case of the more general problem of evaluating the functional derivative of implicit density functionals.

While OEP implementations employing fully numerical calculations on real-space grids are available (see, e.g., Refs. 40 and 41), their applicability is currently limited to benchmark calculations for atoms and diatomic molecules. Thus, for applying OEP methods to many-electron systems and large molecules, the orbitals have to be expanded in finite basis sets. The introduction of a finite orbital basis set, however, turns the OEP method into an ill-posed problem and the solution becomes non-unique.<sup>42</sup> This ill-posed nature is common to many inverse problems and makes the inverse mapping from an electron density to a local potential unstable and sensitive to optimization parameters. Furthermore, these

<sup>a)</sup>Authors to whom correspondence should be addressed. Electronic addresses: christoph.jacob@kit.edu and markus.reiher@phys.chem.ethz.ch.

drawbacks result in unphysical potentials, which can contain large oscillations affecting orbital energies and derived properties.<sup>42,43</sup>

To allow for a routine application of the OEP method in quantum chemistry approaches to regularize the OEP solutions have been proposed. One approach developed by Heßelmann *et al.*<sup>44</sup> is based on explicitly constructing an orbital basis set that is balanced with respect to the basis set employed for expanding the potential, whereas the orbital basis set is balanced implicitly in the approach of Kollmar and Filatov.<sup>45,46</sup> However, these methods require very large orbital basis sets, which hampers their application to larger molecular systems. A different approach was developed by Yang and co-workers,<sup>43,47</sup> who introduced a regularization parameter in the energy functional to make the resulting optimized potentials as smooth as possible. Recently, an approach which yields unambiguous potentials for any combination of orbital and potential basis sets and that provides high-quality potentials already with small orbital basis sets was suggested by one of us.<sup>48</sup> It is based on the condition that the optimal reconstructed potential should yield the target density when extending the orbital basis set.

So far, OEP methods for reconstructing the xc potential from accurate *ab initio* densities have mainly been applied to closed-shell systems, i.e., to the total electron density as target only (for exceptions, see Refs. 32 and 49). For open-shell systems, one commonly employs an unrestricted KS-DFT formalism,<sup>1,50,51</sup> in which the spin polarization density  $Q(\mathbf{r}) = \rho^\alpha(\mathbf{r}) - \rho^\beta(\mathbf{r})$  is used as an additional fundamental variable. This leads to separate KS equations for  $\alpha$ - and  $\beta$ -electrons containing different xc potentials  $v_{\text{xc}}^\alpha[\rho, Q] = \delta E_{\text{xc}}[\rho, Q]/\delta\rho_\alpha$  and  $v_{\text{xc}}^\beta[\rho, Q] = \delta E_{\text{xc}}[\rho, Q]/\delta\rho_\beta$ , i.e., the  $\alpha$ - and  $\beta$ -electron densities  $\rho^\alpha(\mathbf{r})$  and  $\rho^\beta(\mathbf{r})$ , respectively, are determined separately. In the following, we will refer to  $Q(\mathbf{r})$  as spin density, to distinguish it from the spin polarization  $\xi(\mathbf{r}) = Q(\mathbf{r})/\rho(\mathbf{r})$  often used in the DFT literature.<sup>1</sup> To denote  $Q(\mathbf{r})$  as spin density is also common in the discussion of electron spin resonance experiments<sup>52</sup> and in texts on spin in quantum chemistry<sup>53,54</sup> as well as in density-functional theory<sup>51</sup> and related approaches.<sup>55</sup> We note that sometimes the term spin density is also used for the individual  $\rho^\alpha(\mathbf{r})$  and  $\rho^\beta(\mathbf{r})$ .<sup>4</sup> To avoid confusion, we will use  *$\alpha$ -electron density* and  *$\beta$ -electron density* for  $\rho^\alpha(\mathbf{r})$  and  $\rho^\beta(\mathbf{r})$ , respectively, in the following.

In such an unrestricted KS-DFT formalism, the exact spin-resolved xc functional would yield—in addition to the exact total electron density—also the exact spin density.<sup>51,56,57</sup> While the total electron density is determined by the total xc potential

$$v_{\text{xc}}^{\text{tot}}[\rho, Q] = \frac{\delta E_{\text{xc}}[\rho, Q]}{\delta\rho(\mathbf{r})} = \frac{1}{2}(v_{\text{xc}}^\alpha[\rho, Q] + v_{\text{xc}}^\beta[\rho, Q]), \quad (1)$$

the spin density in unrestricted KS-DFT is determined by the spin xc potential<sup>51</sup>

$$v_{\text{xc}}^{\text{spin}}[\rho, Q] = \frac{\delta E_{\text{xc}}[\rho, Q]}{\delta Q(\mathbf{r})} = \frac{1}{2}(v_{\text{xc}}^\alpha[\rho, Q] - v_{\text{xc}}^\beta[\rho, Q]). \quad (2)$$

The former appears in the minimization of the total energy with respect to  $\rho(\mathbf{r})$ , whereas the latter appears in the minimization with respect to  $Q(\mathbf{r})$ .<sup>51</sup> Thus, for improving the spin-density dependence of approximate xc potentials, it would be desirable to be able to reconstruct this spin xc potential  $v_{\text{xc}}^{\text{spin}}[\rho_0, Q_0]$  from accurate *ab initio* total and spin densities. We note that for a given spin state [i.e., an eigenstate of  $\hat{S}^2$  with eigenvalue  $S(S+1)$ ], the spin density depends on the chosen value of  $M_S = -S, \dots, +S$  (i.e., the eigenvalue of  $\hat{S}_z$ )<sup>51</sup> and is given by  $Q^{M_S}(\mathbf{r}) = (M_S/S)Q^{M_S=S}(\mathbf{r})$ . Here, we will focus on the case  $M_S = S$ , as it is commonly considered in KS-DFT, and because it is the only one that is described adequately by the currently available xc functionals.<sup>58,59</sup> For other values of  $M_S$ , the total and spin xc potentials differ, because in unrestricted KS-DFT the xc energy depends on  $M_S$ .<sup>51</sup>

A reconstruction of the spin xc potential  $v_{\text{xc}}^{\text{spin}}[\rho_0, Q_0]$  from accurate *ab initio* (spin) densities has not been attempted previously. When using finite orbital basis sets, such a reconstruction of  $v_{\text{xc}}^{\text{spin}}[\rho_0, Q_0]$  is particularly challenging, as it will be more sensitive to numerical errors than a reconstruction of the total or the individual  $\alpha$ - and  $\beta$ -electron potentials. Here, we extend the unambiguous potential reconstruction developed in Ref. 48 to the spin-unrestricted case. This requires numerical enhancements of our implementation prompted by the use of Gaussian-type orbitals (GTOs) for expanding the orbitals in such wave-function based calculations. Even though the reconstruction algorithm of Ref. 48 can be applied to the spin-unrestricted case without significant modifications, for employing it for the reconstruction of spin potentials its accuracy needs to be assessed carefully, if possible by comparison to reference potentials reconstructed in fully numerical calculations. Thus, the reconstruction of spin potentials can serve as an additional verification of the quality of the potentials reconstructed with the algorithm of Ref. 48.

This work is organized as follows. Section II briefly reviews the potential reconstruction algorithm and outlines its extension to the spin-unrestricted case. In Sec. III, the computational methodology and extensions of our implementation are described. Subsequently, we study the reconstructed xc potentials for two test cases, the lithium atom and the O<sub>2</sub> molecule, in Sec. IV. Here, target densities from both KS-DFT calculations and from accurate wave-function based *ab initio* calculations (full configuration interaction (Full-CI) and complete active space self-consistent field (CASSCF)) are employed. Finally, our conclusions are summarized in Sec. V.

## II. THEORETICAL BACKGROUND

### A. Determining optimized unrestricted Kohn–Sham potentials

Within spin-unrestricted KS-DFT, the wavefunction of the KS reference system is given by a (spin-unrestricted)  $N$ -electron Slater determinant, which is constructed from  $N = N^\alpha + N^\beta$  orthonormal one-particle functions  $\{\phi_i^\sigma(\mathbf{r})\sigma(s), \sigma = \alpha, \beta\}$ . The corresponding spatial orbitals  $\phi_i^\sigma(\mathbf{r})$  can then be determined by solving two separate

sets of one-electron equations<sup>51</sup>

$$\begin{aligned} \left[ -\frac{1}{2}\Delta + v_s^\alpha[\rho, Q](\mathbf{r}) \right] \phi_i^\alpha(\mathbf{r}) &= \varepsilon_i^\alpha \phi_i^\alpha(\mathbf{r}) \quad \text{and} \\ \left[ -\frac{1}{2}\Delta + v_s^\beta[\rho, Q](\mathbf{r}) \right] \phi_i^\beta(\mathbf{r}) &= \varepsilon_i^\beta \phi_i^\beta(\mathbf{r}), \end{aligned} \quad (3)$$

where the  $\alpha$ - and  $\beta$ -electron KS potentials are given by

$$v_s^\sigma[\rho, Q](\mathbf{r}) = v_{\text{nuc}}(\mathbf{r}) + v_{\text{Coul}}[\rho](\mathbf{r}) + v_{\text{xc}}^\sigma[\rho, Q](\mathbf{r}), \quad (4)$$

with the nuclear potential  $v_{\text{nuc}}(\mathbf{r})$ , the Coulomb potential  $v_{\text{Coul}}[\rho](\mathbf{r}) = \int \rho(\mathbf{r}')/|\mathbf{r} - \mathbf{r}'| d^3 r'$ , and the xc potential  $v_{\text{xc}}^\sigma[\rho, Q](\mathbf{r}) = \delta E_{\text{xc}}[\rho, Q]/\delta \rho^\sigma(\mathbf{r})$ . The  $\alpha$ - and  $\beta$ -electron densities are then obtained from the KS orbitals  $\{\phi_i^\sigma\}$  as

$$\rho^\alpha(\mathbf{r}) = \sum_i^{N^\alpha} |\phi_i^\alpha(\mathbf{r})|^2 \quad \text{and} \quad \rho^\beta(\mathbf{r}) = \sum_i^{N^\beta} |\phi_i^\beta(\mathbf{r})|^2. \quad (5)$$

Here, we consider the inverse problem of determining the spin-resolved KS potential [i.e., the local potentials  $v_s^\alpha(\mathbf{r})$  and  $v_s^\beta(\mathbf{r})$ ] from given  $\alpha$ - and  $\beta$ -electron target densities,  $\rho_0^\alpha(\mathbf{r})$  and  $\rho_0^\beta(\mathbf{r})$ , that is, we require

$$\rho^\alpha(\mathbf{r}) = \rho_0^\alpha(\mathbf{r}) \quad \text{and} \quad \rho^\beta(\mathbf{r}) = \rho_0^\beta(\mathbf{r}). \quad (6)$$

An alternative way of expressing this problem is to consider the total and spin densities,<sup>51</sup>

$$\rho(\mathbf{r}) = \rho^\alpha(\mathbf{r}) + \rho^\beta(\mathbf{r}) \quad \text{and} \quad Q(\mathbf{r}) = \rho^\alpha(\mathbf{r}) - \rho^\beta(\mathbf{r}) \quad (7)$$

as target, and to regard the total and spin potentials,<sup>51</sup>

$$\begin{aligned} v_s^{\text{tot}}(\mathbf{r}) &= \frac{1}{2} (v_s^\alpha(\mathbf{r}) + v_s^\beta(\mathbf{r})) \quad \text{and} \\ v_s^{\text{spin}}(\mathbf{r}) &= \frac{1}{2} (v_s^\alpha(\mathbf{r}) - v_s^\beta(\mathbf{r})) \end{aligned} \quad (8)$$

as the quantities that are sought. Here, the total KS potential

$$v_s^{\text{tot}}[\rho, Q](\mathbf{r}) = v_{\text{nuc}}(\mathbf{r}) + v_{\text{Coul}}[\rho](\mathbf{r}) + v_{\text{xc}}^{\text{tot}}[\rho, Q](\mathbf{r}) \quad (9)$$

is the component determining the total electron density, whereas the spin KS potential

$$v_s^{\text{spin}}[\rho, Q](\mathbf{r}) = v_{\text{xc}}^{\text{spin}}[\rho, Q](\mathbf{r}) = \frac{\delta E_{\text{xc}}[\rho, Q]}{\delta Q(\mathbf{r})} \quad (10)$$

determines the spin density. Therefore, this representation will be particularly useful for understanding the dependence of the xc potential on the spin density  $Q(\mathbf{r})$  and to identify the reason for the failure of approximate xc functionals to describe the spin density correctly in some cases.<sup>15</sup>

In principle, any method applicable for reconstructing the KS-potential in closed-shell systems could be adapted to the spin-unrestricted case by applying it separately to the  $\alpha$ - and  $\beta$ -electron densities. However, already the closed-shell cases poses many numerical difficulties, and achieving uniform accuracy for the  $\alpha$ - and  $\beta$ -spin potentials, as it is required for obtaining  $v_s^{\text{spin}}(\mathbf{r})$  accurately, turns out to be a challenging task.

The conceptually simplest approach for determining the local potential yielding a given target density is to represent the potential numerically on a grid and to determine it iteratively. Several methods working along these lines have

been developed over the past decades.<sup>16,60–63</sup> Generally, these methods calculate the density from some trial potential and then update the potential by comparing the density to the target density. If the density is too large at a grid point, the potential is made more repulsive at this point. Conversely, if the density is too small, the potential is made more attractive. This process is repeated iteratively until the target density is obtained. Different numerical potential reconstruction methods differ in the way in which the potential is updated in each iteration.<sup>16,62,63</sup> The only exception is the method of Zhao–Morrison–Parr,<sup>61</sup> which uses a conceptually different approach.

However, such numerical methods also require that the KS equations [Eq. (3)] are solved numerically on the same grid. Therefore, their application has mainly been limited to (closed-shell) atoms and, in some cases, (closed-shell) diatomic molecules.<sup>64,65</sup> Here, we will employ such a fully numerical scheme to obtain accurate reference potentials for atoms. For determining optimized KS potentials in general molecular systems, both the orbitals and the potential are usually expanded in a basis set.<sup>37,39</sup> However, as will be discussed below, with finite orbital basis sets the potential reconstruction turns into an ill-posed problem, in which the resulting potential is not unique.<sup>42,43,66</sup>

To overcome the resulting numerical difficulties, we will apply the recently developed unambiguous optimization method<sup>48</sup> and generalize it to unrestricted KS potentials. This scheme is based on a two-step procedure, in which one first determines a non-unique potential using a direct optimization in a finite basis set. Subsequently, an unambiguous optimized potential is singled out by means of a suitable criterion.

## B. Direct optimization of unrestricted Kohn–Sham potentials

In the first step, two non-unique local potentials  $v_s^\alpha(\mathbf{r})$  and  $v_s^\beta(\mathbf{r})$  yielding the target  $\alpha$ - and  $\beta$ -electron densities  $\rho_0^\alpha(\mathbf{r})$  and  $\rho_0^\beta(\mathbf{r})$ , respectively, in a given finite basis set have to be determined. To this end, we apply the direct optimization method by Wu and Yang (WY)<sup>39</sup> and extend it to the spin-unrestricted case.

The KS kinetic energy for any pair of  $\alpha$ - and  $\beta$ -electron densities  $\rho_0^\alpha, \rho_0^\beta$  is defined as<sup>1,67</sup>

$$T_s[\rho_0^\alpha, \rho_0^\beta] = \min_{\Psi_s \rightarrow \rho_0^\alpha, \rho_0^\beta} \langle \Psi_s | \hat{T} | \Psi_s \rangle = \frac{1}{2} T_s[2\rho_0^\alpha] + \frac{1}{2} T_s[2\rho_0^\beta], \quad (11)$$

where  $\hat{T} = -\Delta/2$  is the kinetic-energy operator and where the minimization includes all wavefunctions  $\Psi_s$  corresponding to a spin-unrestricted  $N$ -electron Slater determinant with  $\alpha$ - and  $\beta$ -electron densities  $\rho^\alpha(\mathbf{r})$  and  $\rho^\beta(\mathbf{r})$ . Hence,  $T_s[\rho_0^\alpha, \rho_0^\beta]$  corresponds to the minimum kinetic energy of an unrestricted KS wave function  $\Psi_s$  under the constraint that its  $\alpha$ - and  $\beta$ -electron densities equal the target densities.<sup>68,69</sup>

The constraint minimization problem of Eq. (11) can be reduced to two separate problems for  $2\rho^\alpha$  and  $2\rho^\beta$ , respectively, which results in two Lagrangian functionals,  $W^\alpha[\rho^\alpha(\mathbf{r})]$  and  $W^\beta[\rho^\beta(\mathbf{r})]$ , subject to the constraints of

Eq. (6) with two corresponding Lagrangian multiplier functions,  $v_s^\alpha(\mathbf{r})$  and  $v_s^\beta(\mathbf{r})$ ,

$$W^\sigma[v_s^\sigma] = \sum_i^{N^\sigma} \langle \phi_i^\sigma | \hat{T} | \phi_i^\sigma \rangle + \int v_s^\sigma(\mathbf{r}) (\rho^\sigma(\mathbf{r}) - \rho_0^\sigma(\mathbf{r})) d^3r \quad \text{for } \sigma = \alpha, \beta. \quad (12)$$

Following Ref. 39, the local potentials which yield the target  $\alpha$ - and  $\beta$ -electron densities can now be determined by the unconstrained maximization of  $W^\sigma[\rho^\sigma(\mathbf{r})]$  with respect to the local potential  $v_s^\sigma(\mathbf{r})$  for each electron spin  $\sigma$ .

To perform this maximization, the local potential is expanded in a finite basis set as<sup>38,39</sup>

$$v_s^\sigma(\mathbf{r}) = v_{\text{ext}}(\mathbf{r}) + v_{\text{Coul}}[\rho_0](\mathbf{r}) + v_0(\mathbf{r}) + \sum_t b_t^\sigma g_t(\mathbf{r}), \quad (13)$$

where  $v_{\text{nuc}}(\mathbf{r})$  is the nuclear potential,  $v_{\text{Coul}}(\mathbf{r})$  is the Coulomb potential of the target density  $\rho_0 = \rho_0^\alpha + \rho_0^\beta$ , and  $v_0(\mathbf{r})$  represents an initial guess for the xc potential, while the remainder is expressed as a linear combination of a finite set of basis functions  $\{g_t(\mathbf{r})\}$  with coefficients  $\{b_t^\sigma\}$ . For fixed  $v_{\text{ext}}(\mathbf{r})$  and  $v_0(\mathbf{r})$ , the unconstrained maximization of  $W^\sigma[v^\sigma]$  turns into an extremum problem with respect to the expansion coefficients  $\{b_t^\sigma\}$  for each electron spin. The first and second derivatives of  $W^\sigma[\rho^\sigma(\mathbf{r})]$  with respect to  $\{b_t^\sigma\}$  can be calculated analytically and one obtains<sup>39</sup> the following expression for the gradient:

$$\frac{\partial W^\sigma}{\partial b_t^\sigma} = \int g_t(\mathbf{r}) (\rho^\sigma(\mathbf{r}) - \rho_0^\sigma(\mathbf{r})) d^3r \quad (14)$$

and the Hessian,

$$H_{st} = \frac{\partial^2 W^\sigma}{\partial b_s^\sigma \partial b_t^\sigma} = 2 \sum_i^{\text{occ}^\sigma} \sum_a^{\text{unocc}^\sigma} \frac{\langle \phi_i^\sigma | g_s | \phi_a^\sigma \rangle \langle \phi_a^\sigma | g_t | \phi_i^\sigma \rangle}{\epsilon_i^\sigma - \epsilon_a^\sigma}, \quad (15)$$

for each electron spin  $\sigma$ . Note that Eqs. (14) and (15) are simplified for the case of real-valued orbitals here. With the gradient and Hessian available, the maximization can be performed using a standard Newton–Raphson optimization.

If a finite basis sets is employed for representing the KS orbitals, the potential reconstruction turns into an ill-posed problem and the optimized potentials resulting from the WY direct optimization as described here are not unique.<sup>42,43,66</sup> This can be seen<sup>48</sup> by considering a change in the local  $\alpha$ - or  $\beta$ -electron potential  $\Delta v_s^\sigma(\mathbf{r}) = v_s^\sigma(\mathbf{r}) - v_{s,0}^\sigma(\mathbf{r})$ , where  $v_{s,0}^\sigma(\mathbf{r})$  is the potential obtained from the direct optimization, generating the orbitals  $\{\phi_i^\sigma\}$  and  $\{\phi_a^\sigma\}$ . To first order, this change  $\Delta v_s^\sigma(\mathbf{r})$  induces a response in the density

$$\Delta \rho^\sigma(\mathbf{r}) = 2 \sum_i^{\text{occ}^\sigma} \sum_a^{\text{unocc}^\sigma} \frac{\langle \phi_a^\sigma | \Delta v_s^\sigma | \phi_i^\sigma \rangle}{\epsilon_i^\sigma - \epsilon_a^\sigma} \phi_i^\sigma(\mathbf{r}) \phi_a^\sigma(\mathbf{r}), \quad (16)$$

with  $\Delta v^\sigma(\mathbf{r}) = \sum_t \Delta b_t^\sigma g_t(\mathbf{r})$  and  $\Delta b_t^\sigma = b_t^\sigma - b_{t,0}^\sigma$ . Here, one notices that any change in the potential  $\Delta v_s^\sigma(\mathbf{r})$  will leave the electron density unchanged if  $\langle \phi_a^\sigma | \Delta v_s^\sigma | \phi_i^\sigma \rangle = 0$ . Hence, if the orbital basis is not flexible enough, the  $\alpha$ - and  $\beta$ -electron densities are not affected by certain changes, e.g., oscillations, in the respective potentials. Linear combinations of basis functions  $g_t(\mathbf{r})$  for which the condition  $\langle \phi_a^\sigma | \Delta v_s^\sigma | \phi_i^\sigma \rangle = 0$  holds are obtained by inserting the basis set expansion for

the potential and performing a singular value decomposition (SVD) of the matrix  $B_{ai,t}^\sigma = \langle \phi_a^\sigma | \phi_i^\sigma | g_t \rangle / (\epsilon_i^\sigma - \epsilon_a^\sigma)$ , which leads to

$$\Delta \rho^\sigma(\mathbf{r}) = 2 \sum_r s_r^\sigma \Delta \tilde{b}_r^\sigma \tilde{\Phi}_r^\sigma(\mathbf{r}), \quad (17)$$

where  $\{s_r^\sigma\}$  are the singular values of  $\mathbf{B}^\sigma$  and where  $\Delta \tilde{b}_r^\sigma = \sum_t V_{t,r}^\sigma \Delta b_t^\sigma$  and  $\tilde{\Phi}_r^\sigma(\mathbf{r}) = \sum_{ia} U_{ia,r}^\sigma \phi_a^\sigma(\mathbf{r}) \phi_i^\sigma(\mathbf{r})$  are the expansion coefficients of the change in the potential and the occupied–virtual orbital products transformed with the left and right singular vectors,  $(V_{t,r}^\sigma)$  and  $(U_{ia,r}^\sigma)$ , respectively. Here, the transformed expansion coefficients  $\tilde{b}_r^\sigma$  refer to the transformed potential basis functions  $\tilde{g}_r^\sigma(\mathbf{r}) = \sum_t V_{t,r}^\sigma g_t(\mathbf{r})$ . Thus, we notice that if one of these transformed potential basis functions  $\tilde{g}_r^\sigma(\mathbf{r})$  corresponds to a singular value  $s_r$  that is zero or very small, the corresponding expansion coefficient  $\tilde{b}_r^\sigma(\mathbf{r})$  can be changed (almost) freely without affecting the density. Therefore, an additional criterion is necessary for singling out the optimal optimized potential among those yielding the same density within the finite basis set.

### C. Choosing the optimal optimized potential

One possibility for unambiguously singling out an optimized potential was suggested in Ref. 48. This scheme starts from the requirement that the optimized potential obtained with a finite orbital basis set should be as close as possible to the one obtained in the basis set limit. Specifically, the density calculated from the optimal optimized potential should still agree with the target density  $\rho_0^\alpha(\mathbf{r})$  or  $\rho_0^\beta(\mathbf{r})$ . Thus, we introduce a complete set of virtual orbitals (see Ref. 48 for details),

$$\tilde{\phi}_r^\sigma(\mathbf{r}') = \delta(\mathbf{r} - \mathbf{r}') - \sum_j^{\text{occ}^\sigma} \phi_j^\sigma(\mathbf{r}') \phi_j^\sigma(\mathbf{r}), \quad (18)$$

with the Dirac delta function  $\delta(\mathbf{r} - \mathbf{r}')$  and where the second term ensures the orthogonality of  $\tilde{\phi}_r^\sigma(\mathbf{r}')$  and the occupied orbitals  $\phi_i^\sigma(\mathbf{r})$ . With this complete representation of the virtual orbital space, the change in the electron density due to a variation in the potential [Eq. (16)] can be approximated as

$$\Delta \rho^\sigma(\mathbf{r}) \approx \sum_i^{\text{occ}^\sigma} \phi_i^\sigma(\mathbf{r}) \langle \tilde{\phi}_r^\sigma | \hat{T} + v_s^\sigma | \phi_i^\sigma \rangle. \quad (19)$$

For singling out the optimal potential, we search for the potential for which the electron density does not change considerably when the orbital basis is enlarged, and minimize

$$\int \frac{\Delta \rho(\mathbf{r})^2}{\rho(\mathbf{r})} d^3r \approx \int \frac{1}{\rho^\sigma(\mathbf{r})} \left[ \sum_i^{\text{occ}^\sigma} \phi_i^\sigma(\mathbf{r}) \langle \tilde{\phi}_r^\sigma | \hat{T} + v_s^\sigma | \phi_i^\sigma \rangle \right]^2 \times d^3r \rightarrow \min. \quad (20)$$

Here, the inverse density has been introduced as a weighting function (i.e., the relative change in the density is minimized) to obtain a uniformly accurate potential. As is discussed in Ref. 48, this choice can also be justified using theoretical arguments. The minimization then leads to the linear systems of

equations  $\mathbf{A}^\sigma \Delta \mathbf{b}^\sigma = -\mathbf{z}^\sigma$  with<sup>48</sup>

$$A_{st} = \sum_{ij}^{\text{occ}} \int \frac{\phi_i^\sigma(\mathbf{r})\phi_j^\sigma(\mathbf{r})}{\rho^\sigma(\mathbf{r})} \langle \tilde{\phi}_r^\sigma | \tilde{g}_s^\sigma | \phi_i^\sigma \rangle \langle \tilde{\phi}_r^\sigma | \tilde{g}_t^\sigma | \phi_j^\sigma \rangle d^3r \quad (21)$$

and

$$z_t^\sigma = \sum_{ij}^{\text{occ}} \int \frac{\phi_i^\sigma(\mathbf{r})\phi_j^\sigma(\mathbf{r})}{\rho^\sigma(\mathbf{r})} \langle \tilde{\phi}_r^\sigma | \hat{h}_0^\sigma | \phi_i^\sigma \rangle \langle \tilde{\phi}_r^\sigma | \tilde{g}_t^\sigma | \phi_j^\sigma \rangle d^3r, \quad (22)$$

where  $\hat{h}_0^\sigma = -\Delta/2 + v_s^\sigma(\mathbf{r})$ . This problem can be solved directly, without explicitly solving the KS equations using an extended orbital basis set. Results obtained using this scheme will be referred to as “optimal (full)” in the following.

For comparison, we will also employ two additional schemes for singling out one optimized potential. The first one, called “balanced” in the following, is based on the idea that a unique potential is also obtained if the potential basis set is chosen such that it is balanced with respect to the orbital basis set.<sup>44</sup> This can be achieved by only retaining those transformed potential basis functions  $\tilde{g}_r^\sigma(\mathbf{r})$  corresponding to singular values  $s_r$  that are not too small, i.e., above a chosen threshold  $s_{\text{thr}}$ . This is closely related to the OEP scheme of Kollmar and Filatov.<sup>45</sup> Note that in the spin-unrestricted case considered here, such a scheme effectively employs different potential basis sets for the  $\alpha$ - and  $\beta$ -spin potentials.

In addition, we also use a criterion for singling out the optimized potentials that are as smooth as possible (labelled “smooth” in the following). To this end, we minimize the norm of the gradient of the potential,

$$\int |\nabla v_s^\sigma(\mathbf{r})|^2 d^3r = \int \left[ \sum_t b_t^\sigma \nabla g_t^\sigma(\mathbf{r}) \right]^2 d^3r \rightarrow \min, \quad (23)$$

under the constraint that the change in the density [Eq. (17)] is below a chosen threshold  $e_{\text{thr}}$ . This results in a quadratic programming problem that can be solved using standard approaches.<sup>48</sup> This criterion is in close analogy to the method of Yang and co-workers,<sup>43,47,70</sup> who introduced a similar constraint by employing a penalty function during the direct optimization. Note that a common feature of all three approaches presented here is that they are applied *a posteriori*, and hence a direct optimization of the potentials must be performed first. This first step then provides a non-unique potential and corresponding orbitals, which are required for the following second step.

### III. COMPUTATIONAL METHODOLOGY

All finite basis set calculations were performed with a local version of the Amsterdam Density Functional (ADF) program package<sup>71</sup> together with the PYADF scripting framework.<sup>72</sup> To allow for the treatment of spin-unrestricted target densities, we extended our recent implementation<sup>31</sup> of the WY direct optimization algorithm and of the subsequent step for singling out an unambiguous optimized potential.<sup>48</sup>

The TZ2P and QZ4P Slater-type orbital (STO) basis sets of ADF were used as orbital basis. The potential was expanded in a finite basis set [Eq. (13)], using ADFs density fitting basis sets corresponding to the TZ2P or QZ4P

orbital basis sets. In all calculations, these basis sets were augmented with additional 1s functions in an even-tempered fashion (see supplementary material<sup>73</sup> for details). As initial guess for the potential, we used a scaled version of the Fermi–Amaldi potential<sup>48,61</sup> of the fixed target electron density  $\rho_0(\mathbf{r}) = \rho_0^\alpha(\mathbf{r}) + \rho_0^\beta(\mathbf{r})$ , namely,

$$v_0(\mathbf{r}) = v_{\text{FA}}[\rho_0](\mathbf{r}) = -\frac{\xi}{N} \int \frac{\rho_0(\mathbf{r}')}{|\mathbf{r} - \mathbf{r}'|} d^3r', \quad (24)$$

where  $\xi$  represents the most diffuse exponent in the STO orbital basis set. This scaled Fermi–Amaldi potential ensures that the optimized local potentials have the correct long-range behavior. In the case of target densities obtained from wavefunction based *ab initio* calculations, which employed GTO basis sets, the Coulomb potential  $v_{\text{Coul}}[\tilde{\rho}_0]$  and Fermi–Amaldi potential  $v_{\text{FA}}[\tilde{\rho}_0]$  in Eq. (13) are evaluated for an approximate reference density  $\tilde{\rho}_0(\mathbf{r})$  obtained from a DFT calculation in ADF in which the orbitals are expanded in STO basis functions.

If large basis sets are employed for the potential, the Hessian matrix of Eq. (15) contains many small eigenvalues which decay gradually to zero. This causes convergence problems during the Newton–Raphson optimization, which we previously addressed by ignoring eigenvalues below a certain threshold. However, for *ab initio* target densities expanded in GTOs, this scheme still caused poor convergence behavior. Therefore, we followed the work of Wu and Yang<sup>74</sup> and performed a SVD of the Hessian  $\mathbf{H}$ . Then the inverse Hessian can be expressed as

$$\mathbf{H}^{-1} = \mathbf{U} \text{diag}(1/\sigma_r) \mathbf{V}^T, \quad (25)$$

where the columns of  $\mathbf{U}$  and  $\mathbf{V}$  are the left and right singular vectors, respectively, for the corresponding singular values  $\sigma_r$ . To this inverse Hessian, a Tikhonov regularization<sup>75,76</sup> is applied by replacing it by

$$\mathbf{H}^{-1} = \mathbf{U} \text{diag}(f_r/\sigma_r) \mathbf{V}^T, \quad (26)$$

where  $f_r$  is a filter factor, which is chosen as

$$f_r = \frac{\sigma_r^2}{\sigma_r^2 + \lambda^2}. \quad (27)$$

We found that appropriate values for the parameter  $\lambda$  turn out to be  $10^{-4} \leq \lambda \leq 0.01$ . If  $\sigma_r \gg \lambda$ , the filter factor  $f_r$  is approximately one, while in the case of  $\sigma_r \ll \lambda$ ,  $f_r$  approaches zero. Thus, instead of abruptly discarding small singular values, the Tikhonov regularization cuts them off gradually.

As convergence criterion for the WY direct optimization, we used the absolute error in the  $\alpha$ - and  $\beta$ -electron densities  $\Delta_{\text{abs}}$  compared to the target  $\alpha$ - and  $\beta$ -electron densities, defined as

$$\Delta_{\text{abs}}^\sigma = \int |\rho^\sigma(\mathbf{r}) - \rho_0^\sigma(\mathbf{r})| d^3r. \quad (28)$$

The minimal absolute error that can be achieved depends on the considered system, as will be discussed below.

When singling out the optimal potential according to the scheme of Ref. 48, regions in which the electron density is very small turn out to be problematic. This is because for densities expanded in finite GTO or STO basis sets, the exact

potential in these regions shows artifacts caused by unphysical nodes in the density.<sup>77,78</sup> To avoid these artifacts, grid points at which the reconstructed  $\alpha$ - or  $\beta$ -electron densities are smaller than a threshold are ignored when constructing the right-hand side  $\mathbf{z}^\sigma$  according to Eq. (22). This corresponds to assuming that the optimized potentials are already well approximated by the initial guess if the difference between the target and reconstructed density is smaller than the threshold. For the lithium atom, this threshold was chosen as  $10^{-4}$ , whereas for the dioxygen molecule it was set to  $10^{-8}$ .

For target densities expanded in STOs, the xc potential is obtained by adding the Fermi–Amaldi potential to the part of the potential expanded in basis functions [cf. Eq. (13)]. In the case of target densities obtained in GTOs, the final xc potentials for  $\alpha$ - and  $\beta$ -electrons are obtained as

$$v_{\text{xc}}^\sigma(\mathbf{r}) = (v_{\text{Coul}}[\tilde{\rho}_0](\mathbf{r}) - v_{\text{Coul}}[\rho_{\text{WY}}](\mathbf{r})) + v_{\text{FA}}[\tilde{\rho}_0](\mathbf{r}) + \sum_t b_t^\sigma g_t(\mathbf{r}). \quad (29)$$

Here, the first term accounts for the difference between the Coulomb potential used as initial guess (evaluated for the density  $\tilde{\rho}_0$ ) and the Coulomb potential corresponding to the target density  $\rho_0$ . The latter is approximated by the density  $\rho_{\text{WY}}$  obtained in a STO expansion from the WY optimization before singling out an unambiguous potential, as this density represents to the best available STO representation of the GTO target density.

To obtain numerical reference potential for atoms, we employed a modified van Leeuwen–Baerends algorithm<sup>16</sup> in combination with a numerical solution of the KS equations on a logarithmic radial grid,<sup>79,80</sup> as described in Ref. 48. Here,

we used the same initial guess for the potential, and updated the potential iteratively until the absolute errors  $\Delta_{\text{abs}}^\sigma$  compared to the target  $\alpha$ - and  $\beta$ -electron densities were each below  $10^{-4}$  e bohr<sup>-3</sup>.

All CASSCF calculations for obtaining accurate *ab initio* target densities were performed with the MOLPRO program package<sup>81</sup> using Dunning’s cc-pVTZ basis set for all atoms.<sup>82,83</sup> For the lithium atom, all electrons are correlated in all orbitals [corresponding to a Full-CI treatment], while for the oxygen molecule the electron (spin) density from a CAS(12,12)SCF calculation was employed. Here, we verified that the resulting densities are converged with respect to the dimension of the active space.

## IV. OPTIMIZED POTENTIALS FROM SPIN DENSITIES

### A. The lithium atom

#### 1. BP86 target (spin) density expanded in STOs

As a simple test case, we consider the lithium atom. In its doublet ground-state, there are two  $\alpha$ - and one  $\beta$ -electron. First, we use the  $\alpha$ - and  $\beta$ -electron densities from a unrestricted KS-DFT calculation employing the QZ4P orbital basis set and the BP86 xc functional as target. Here, it should be possible to reproduce the target densities accurately if the same orbital basis set is used. The target total and spin densities are shown in Fig. 1. For the lithium atom, there are only minimal differences between the  $\alpha$ - and  $\beta$ -electron orbitals, and the spin density is thus determined by the unpaired electron in the 2s orbital (see also Fig. 1 in the supplementary material<sup>73</sup>).

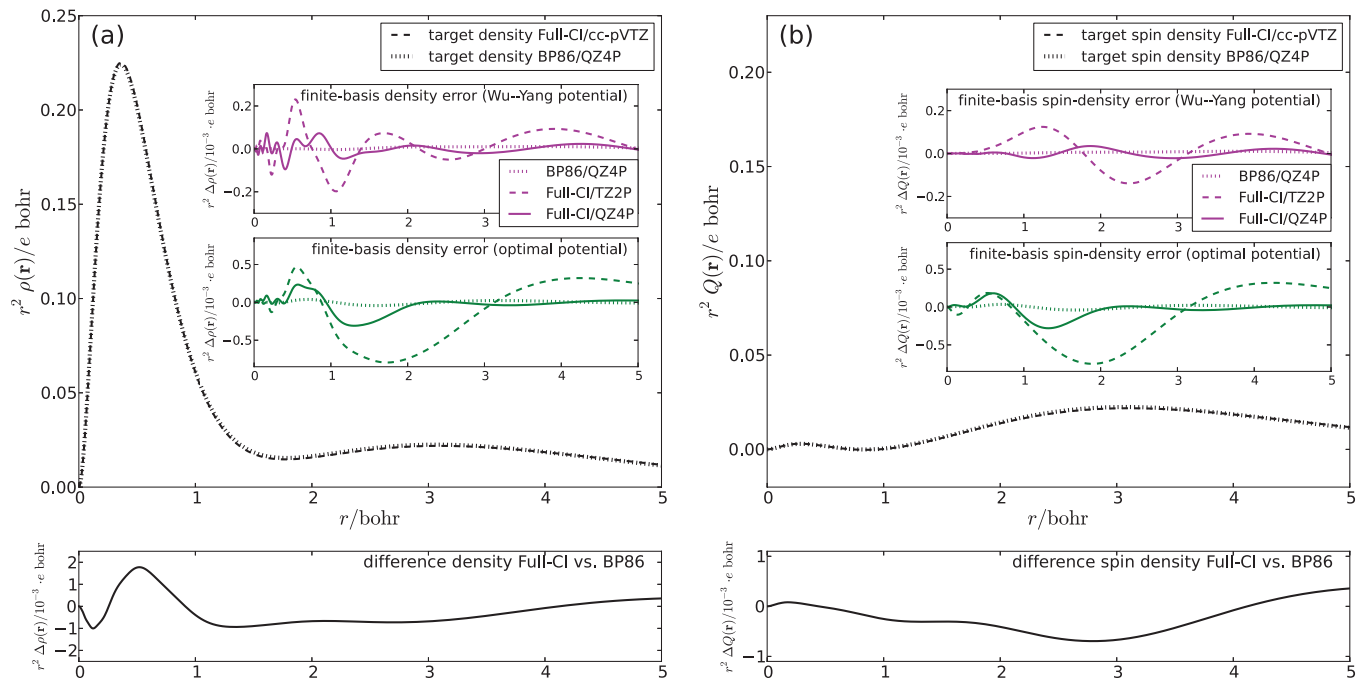


FIG. 1. Target radial (a) total densities and (b) spin densities for the lithium atom obtained from BP86/QZ4P and Full-Cl/cc-pVTZ calculations. The difference between these two target densities is shown in the lower part. The insets present the difference between the target total and spin densities and the corresponding density obtained in the finite orbital basis set from the WY optimized potentials (upper insets) and from the optimal optimized potentials (lower insets). For the Full-Cl/cc-pVTZ results obtained with both the TZ2P and QZ4P orbital basis sets in the potential reconstruction are included. The corresponding plots of the  $\alpha$ - and  $\beta$ -electron densities are given in Fig. 1 in the supplementary material.<sup>73</sup>

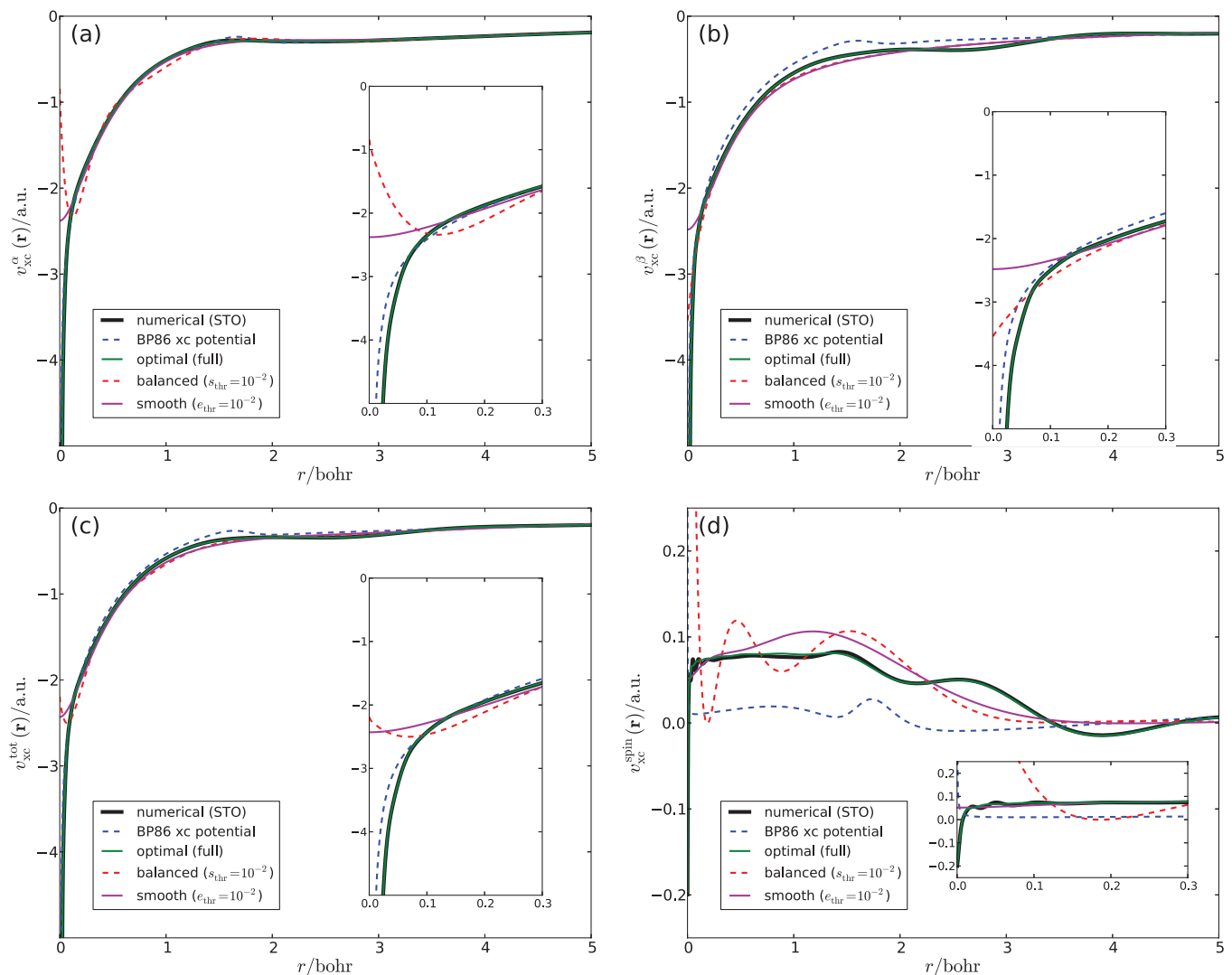


FIG. 2. Reconstructed potentials determined for the Li atom and a BP86/QZ4P target (spin) density. The upper part shows the xc potentials for (a)  $\alpha$  electrons  $v_{xc}^\alpha$  and (b)  $\beta$  electrons  $v_{xc}^\beta$ , while the lower part shows (c) the total xc potential  $v_{xc}^{tot}$  and (d) the spin xc potential  $v_{xc}^{spin}$ . For the potential reconstruction with the finite QZ4P orbital basis set, the potentials obtained with the different schemes for singling out an unambiguous potential (see text for details) are shown. The accurate potentials obtained with a numerical solution of the KS equations (“numerical (STO)”) as well as the BP86 xc potential calculated from the reference density (“BP86 xc potential”) are shown for comparison. The latter is shifted such that it agrees with the numerical reference at  $r = 5$  bohrs.

For assessing the quality of the optimized potentials obtained with finite orbital basis sets, we determined the xc potentials for  $\alpha$ - and  $\beta$ -electrons numerically as described above. These fully numerical potentials are the ones that a finite-basis potential reconstruction should reproduce. They are presented in Fig. 2 as black lines. In addition, the figure includes the BP86 xc potentials evaluated for the target  $\alpha$ - and  $\beta$ -electron densities (blue dashed line), i.e., the potentials that were used in the finite-basis set KS-DFT calculation for determining the target  $\alpha$ - and  $\beta$ -electron densities. We note that, even though it is close to it, these BP86 potentials do not agree with the numerical references. As was pointed out before, they should only be equal in the basis set limit.<sup>48,78</sup>

The reconstructed  $\alpha$ - and  $\beta$ -electron xc potentials  $v_{xc}^\alpha(\mathbf{r})$  and  $v_{xc}^\beta(\mathbf{r})$  obtained with the finite QZ4P orbital basis set are shown in Figs. 2(a) and 2(b). In both cases, the potentials obtained from the WY optimization in the first step show large oscillations and are, therefore, not shown in the figures. These

oscillations are removed if a potential is singled out in the second step. Irrespective of which of the schemes described in Sec. II C is applied, the potentials closely agree with the numerical reference for  $r > 0.5$  bohr. However, differences are found closer to the nucleus. When using an implicitly balanced potential basis set (dashed red line), the potential is too large close to the nucleus and still shows slight oscillations. Singling out the potential that is as smooth as possible (solid magenta line) does not introduce oscillations, but also results in a potential with the wrong behavior for small  $r$ . On the other hand, the optimal potential determined using the criterion of Eq. (20) closely matches the numerical reference potential everywhere.

For a more quantitative comparison of the different approaches, Table I lists the absolute errors  $\Delta_{abs}^{\sigma,\text{num}}$  [cf. Eq. (28)] in the  $\alpha$ - and  $\beta$ -electron densities obtained from the different potentials in a numerical solution of the KS equations. Naturally, this absolute error is the smallest for the numerical

TABLE I. Absolute errors  $\Delta_{\text{abs}}^{\sigma}$  in the  $\alpha$ - and  $\beta$ -electron densities with respect to the target  $\alpha$ - and  $\beta$ -electron densities (in  $\text{e bohr}^{-3}$ ) obtained with different reconstructed potentials for the Li atom with BP86/QZ4P target densities. The QZ4P orbital basis set is used in the finite-basis set potential reconstruction.  $\Delta_{\text{abs}}^{\sigma, \text{finite}}$  refers to the error in the density obtained from the respective potentials in the finite orbital basis set, whereas  $\Delta_{\text{abs}}^{\sigma, \text{num}}$  is the error for the density obtained from a numerical solution of the KS equations.

	$\Delta_{\text{abs}}^{\alpha, \text{num}}$	$\Delta_{\text{abs}}^{\alpha, \text{finite}}$	$\Delta_{\text{abs}}^{\beta, \text{num}}$	$\Delta_{\text{abs}}^{\beta, \text{finite}}$
Numerical (STO)	$<10^{-4}$	0.0007	$<10^{-4}$	0.0001
Wu-Yang	0.0098	0.0008	0.0036	$<10^{-4}$
Balanced ( $s_{\text{thr}} = 10^{-2}$ )	0.0090	0.0024	0.0016	0.0006
Smooth ( $e_{\text{thr}} = 10^{-2}$ )	0.0087	0.0086	0.0082	0.0082
Optimal (full)	0.0009	0.0014	$<10^{-4}$	$<10^{-4}$

reference potential. For the potential obtained from the WY optimization, the error is approximately two orders of magnitude larger. This error is only slightly reduced by using an implicitly balanced basis set or by singling out a smooth potential. In contrast, for the optimal potential, the absolute error in the numerical density is reduced by another order of magnitude. Thus, these results confirm the previous finding that high-quality potentials can be obtained by applying the criterion of Eq. (20) for unambiguously singling out the optimal potential.<sup>48</sup>

In addition to the errors in the numerical densities, Table I also includes the absolute errors  $\Delta_{\text{abs}}^{\sigma, \text{finite}}$  in the densities obtained with the different potentials in the finite orbitals basis set. In this case, the smallest error is obtained for the potentials obtained directly from the WY optimization, and these absolute errors correspond to the convergence criterion used in this step. After singling out one potential in the second step the error increases, but the smallest one is obtained for the optimal potential. Note that for both the optimal and the numerical reference potential the absolute density errors are larger in the finite orbital basis set than for the numerical solution of the KS equations. This discrepancy was discussed previously<sup>48</sup> and arises because it is in general not possible to simultaneously reproduce the target density both in a given finite basis set and in a fully numerical calculation. However, these differences decrease when increasing the size of the orbital basis set.

After assessing the quality of the reconstructed  $\alpha$ - and  $\beta$ -electron xc potentials, we turn to Figs. 2(c) and 2(d), where the same results are shown as total and spin xc potentials, respectively. While for the total potential, the overall results are similar to those discussed for the individual spin components, it is apparent that reconstructing the spin potential accurately is significantly more difficult. For the lithium atom considered here, the difference between the  $\alpha$ - and  $\beta$ -electron orbitals is very small. Therefore, the spin xc potential is very small as well. In particular, it is almost constant in the range probed by the 1s orbital and, therefore, does not introduce a significant difference between the  $\alpha$ - and  $\beta$ -electron 1s orbitals. Hence, the spin potential is mostly due to the different asymptotic decay of the  $\alpha$ - and  $\beta$ -electron densities. Since the BP86 xc potentials evaluated from the target  $\alpha$ - and  $\beta$ -electron densities do not show the correct asymptotic decay, the corresponding spin potential almost vanishes. In contrast, the optimal spin

potential reproduces the numerical reference almost perfectly. Note again that the numerical potential—and not the BP86 xc potential—is the one that the finite-basis potential reconstruction should reproduce. The smooth and the balanced potential deviate from the numerical reference not only close to the nuclei (where these differences were also recognizable for the  $\alpha$ - and  $\beta$ -spin potentials), but also further away from the nuclei. Thus, in order to reconstruct the spin potential  $v_{\text{xc}}^{\text{spin}}(\mathbf{r})$  reliably, it is essential to single out the optimal potential according to the criterion of Eq. (20).

## 2. Full-CI target (spin) density expanded in GTOs

Next, we use the accurate  $\alpha$ - and  $\beta$ -electron densities from a Full-CI calculation for the lithium atom as our target. In this case, the target  $\alpha$ - and  $\beta$ -electron densities have to be expanded in a GTO orbital basis set, which might result in additional difficulties when performing the potential reconstruction with our implementation using a STO orbital basis set. The Full-CI total and spin densities are included in Fig. 1 and are on the scale of the plots almost indistinguishable from the BP86 ones considered above.

Figure 3 shows the reconstructed total and spin xc potentials. We used two different STO orbital basis sets (TZ2P and QZ4P), but only include the QZ4P results in the figure, while the TZ2P potentials are presented in Fig. 2 in the supplementary material.<sup>73</sup> The reference potentials obtained from the Full-CI density with a numerical solution of the KS equations are included as black dashed lines in Fig. 3. These numerical potentials features considerable oscillations which are most pronounced near the nucleus. Such an oscillatory behavior is commonly found when the target density is expanded in GTOs<sup>84</sup> and can be attributed to their deficiency to represent the correct form of the electron density close to the nucleus. However, these oscillations can be reduced when the GTO orbital basis set used for determining the target density is enlarged (see Fig. 3 in the supplementary material<sup>73</sup>).

As a first step of the potential reconstruction, we determine a (non-unique) potential using the WY direct optimization algorithm. For the GTO target densities, looser convergence criteria than for the BP86 target density expanded in STOs have to be used (see Table II). The corresponding difference densities are shown in the upper insets in Fig. 1. Thus, a sufficiently large STO orbital basis set is required to be able to accurately reproduce the target density from an *ab initio* calculation using GTOs. Nevertheless, with the QZ4P basis set it is possible to achieve an agreement close to the one obtained for the target density expanded in STOs. We note that the methodological improvements discussed in Sec. III, in particular, the use of the Tikhonov regularization, are essential here to make this convergence possible.

Since the numerical potential reconstructed from the GTO densities show oscillations due to the insufficiencies of the GTO basis set close to the nucleus, we also performed a numerical potential reconstruction from the  $\alpha$ - and  $\beta$ -electron densities from the WY optimization, which is the closest available approximation of the target densities in STOs. These are included in Fig. 3 as solid black line. They do not show

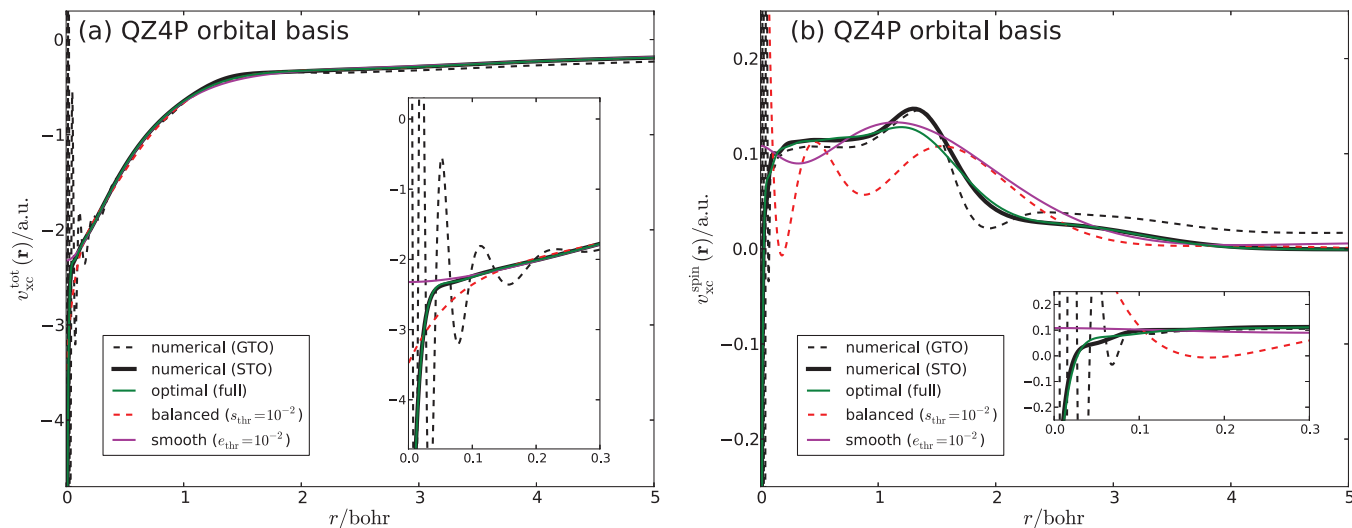


FIG. 3. Reconstructed (a) total xc potentials  $v_{xc}^{\text{tot}}$  and (b) spin xc potentials  $v_{xc}^{\text{spin}}$  determined for the Li atom and a Full-CI/cc-pVTZ target (spin) density with a QZ4P orbital basis set in the potential reconstruction. The accurate potentials obtained with a numerical solution of the KS equations (“numerical (GTO)”) from the GTO target density as well as from the WY reconstructed density (“numerical (STO)”) are shown for comparison. These reference potentials have been shifted such that they agree with the optimal potential at  $r = 2.7$  bohrs. The corresponding plots of the  $\alpha$ - and  $\beta$ -electron potentials are given in Fig. 3 in the supplementary material,<sup>73</sup> and the potentials reconstructed with the TZ2P orbital basis set are shown in Fig. 2 in the supplementary material.<sup>73</sup>

oscillations near the nucleus anymore, but otherwise closely match the numerical potentials reconstructed from the GTO densities. Note, however, that for the TZ2P orbital basis set the total and spin potentials reconstructed from the STO densities show an artifact caused by spurious nodes appearing in the  $\beta$ -electron density in the region where it is very small<sup>77,78</sup> (see Fig. 2 in the supplementary material<sup>73</sup>). In the following, we will consider the numerical potentials reconstructed from the WY densities expanded in the QZ4P STO orbital basis set as reference for the finite-basis set potential reconstruction.

The optimized potentials obtained using the different schemes for singling out one unambiguous potential after the WY optimization are included in Fig. 3. First, we consider the total xc potentials in Figs. 3(a). The total xc potentials from all three schemes closely agree with the numerical reference. Differences only occur for the smooth and balanced potentials close to the nucleus, while the optimal potential matches the reference also in this region. For a more quantitative comparison, the absolute errors  $\Delta_{\text{abs}}^{\sigma,\text{num}}$  in the  $\alpha$ - and  $\beta$ -electron densities obtained from the different potentials in a numerical solution of the KS equations compared to the target  $\alpha$ -

and  $\beta$ -electron densities are listed in Table II. In all cases, the smallest error is achieved for the optimal potential. Moreover, the absolute errors in the numerical densities decrease for all three schemes when going from the TZ2P to the QZ4P orbital basis set.

In addition, Table II includes the absolute errors  $\Delta_{\text{abs}}^{\sigma,\text{finite}}$  in the  $\alpha$ - and  $\beta$ -electron densities obtained with the different potential in the finite orbital basis set. In general, these errors increase compared to the potentials obtained from the WY procedure when applying the schemes for singling out one optimized potential. Again, this is because the error in the finite-basis set density and in the numerical density cannot be minimized at the same time.<sup>48</sup> When going from the TZ2P to the larger QZ4P orbital basis set, the errors decrease significantly, both for the optimal and for the numerical reference potentials. This can also be seen in the corresponding difference densities shown in the lower insets in Fig. 3.

Finally, we turn to the reconstructed spin xc potentials shown in Figs. 3(b) and 3(d). Again, reproducing the numerical reference potential is much more difficult in this case because the spin potential is calculated as the difference of the

TABLE II. Absolute errors  $\Delta_{\text{abs}}^{\sigma}$  in the  $\alpha$ - and  $\beta$ -electron densities with respect to the target  $\alpha$ - and  $\beta$ -electron densities (in  $e \text{ bohr}^{-3}$ ) obtained with different reconstructed potentials for the Li atom and Full-CI/cc-pVTZ target densities. Results obtained both with the TZ2P and with the QZ4P orbital basis set in the potential reconstruction are shown.  $\Delta_{\text{abs}}^{\sigma,\text{finite}}$  refers to the error in the density obtained from the respective potentials in the finite orbital basis set, whereas  $\Delta_{\text{abs}}^{\sigma,\text{num}}$  is the error for the density obtained from a numerical solution of the KS equations.

Full-CI/cc-pVTZ	TZ2P				QZ4P			
	$\Delta_{\text{abs}}^{\alpha,\text{num}}$	$\Delta_{\text{abs}}^{\alpha,\text{finite}}$	$\Delta_{\text{abs}}^{\beta,\text{num}}$	$\Delta_{\text{abs}}^{\beta,\text{finite}}$	$\Delta_{\text{abs}}^{\alpha,\text{num}}$	$\Delta_{\text{abs}}^{\alpha,\text{finite}}$	$\Delta_{\text{abs}}^{\beta,\text{num}}$	$\Delta_{\text{abs}}^{\beta,\text{finite}}$
Numerical (GTO)	<10 <sup>-4</sup>	0.0258	<10 <sup>-4</sup>	0.0086	<10 <sup>-4</sup>	0.0065	<10 <sup>-4</sup>	0.0010
Numerical (STO)	0.0051	0.0158	0.0020	0.0014	0.0025	0.0051	0.0005	0.0005
Wu–Yang	0.0782	0.0051	0.0301	0.0020	0.0165	0.0025	0.0021	0.0004
Balanced ( $s_{\text{thr}} = 10^{-2}$ )	0.0336	0.0079	0.0310	0.0020	0.0092	0.0074	0.0030	0.0004
Smooth ( $e_{\text{thr}} = 10^{-2}$ )	0.0416	0.0105	0.0039	0.0041	0.0120	0.0071	0.0062	0.0061
Optimal (full)	0.0220	0.0284	0.0021	0.0016	0.0061	0.0067	0.0005	0.0006

$\alpha$ - and  $\beta$ -electron potentials. Therefore, even though with the balanced potential agrees with the reference for the total and the individual  $\alpha$ - and  $\beta$ -electron potentials at  $r < 2$  bohrs, the corresponding spin potential deviates significantly and features unphysical oscillations. The smooth spin potential qualitatively reproduces all features of the numerical reference, but the best agreement is again achieved for the optimal potential.

The optimal potentials obtained with the smaller TZ2P orbital basis (see Fig. 2 in the supplementary material<sup>73</sup>) already agree very well with the numerical reference potential determined from the WY density. However, this WY density differs from the target density expanded in GTOs so that deviations to the numerical potential determined from that target density occur. Thus, the QZ4P orbital basis set is required in order to obtain an accurate spin potential not because of the basis set requirements of the scheme for singling out the optimal potential, but because of the need to reproduce the GTO target density with STOs in the WY optimization step. However, the use of a STO representation of the density in the WY step has the advantage of avoiding the spurious oscillations in the reconstructed potential arising for a GTO expansion of the target density close to the nucleus.

Finally, we note that the optimal potentials presented here are converged with respect to the size of the potential basis set. Adding additional tight or diffuse functions does not al-

ter the resulting optimal potentials significantly anymore. The dependence of the optimal potentials on the potential basis set is illustrated in Figs. 5 and 6 and Tables I and II in the supplementary material.<sup>73</sup>

## B. An open-shell molecule: Dioxygen

### 1. BP86 target (spin) density expanded in STOs

We now investigate a diatomic molecule with an open-shell ground state, namely, dioxygen O<sub>2</sub> with an O–O bond distance of 1.21 Å in its equilibrium structure. Here, the two antibonding  $\pi^*$ -orbitals are singly occupied. First, we consider a target density from an unrestricted KS-DFT calculation using the BP86 xc functional and the Slater-type QZ4P orbital basis set. This target spin density is shown along the bonding axis (x axis) and perpendicular to it (y axis) in Figs. 4(a) and 4(b), respectively, and is plotted in the *xy*-plane in Fig. 4(c). Along the y axis, the spin density is determined by the singly occupied orbitals which have a cylindrical shape around the bond axis. On the other hand, the singly occupied orbitals vanish on the bond axis and, therefore, the spin density along the x axis is solely due to the difference between the doubly occupied  $\alpha$ - and  $\beta$ -electron orbitals. In particular,

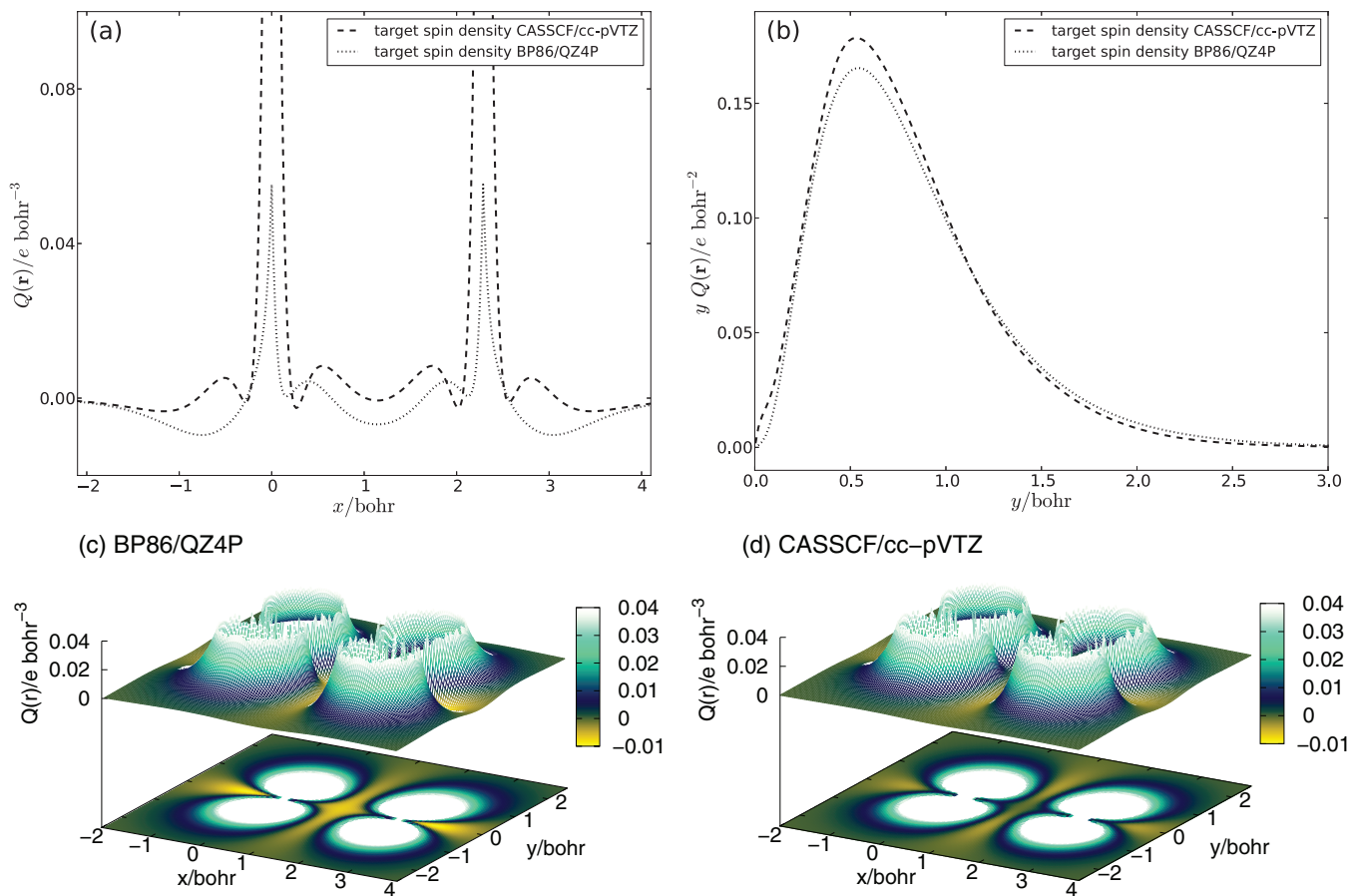


FIG. 4. Target spin densities for the dioxygen molecule obtained from BP86/QZ4P and CAS(12,12)SCF/cc-pVTZ calculations. Both spin densities are compared (a) along the bond axis (x axis), (b) perpendicular to the bond axis (y axis). Furthermore, (c) and (d) show the BP86/QZ4P and CAS(12,12)SCF/cc-pVTZ spin densities, respectively, in the *xy*-plane. The corresponding plots of the total and the individual  $\alpha$ - and  $\beta$ -electron densities are given in Fig. 7 in the supplementary material.<sup>73</sup>

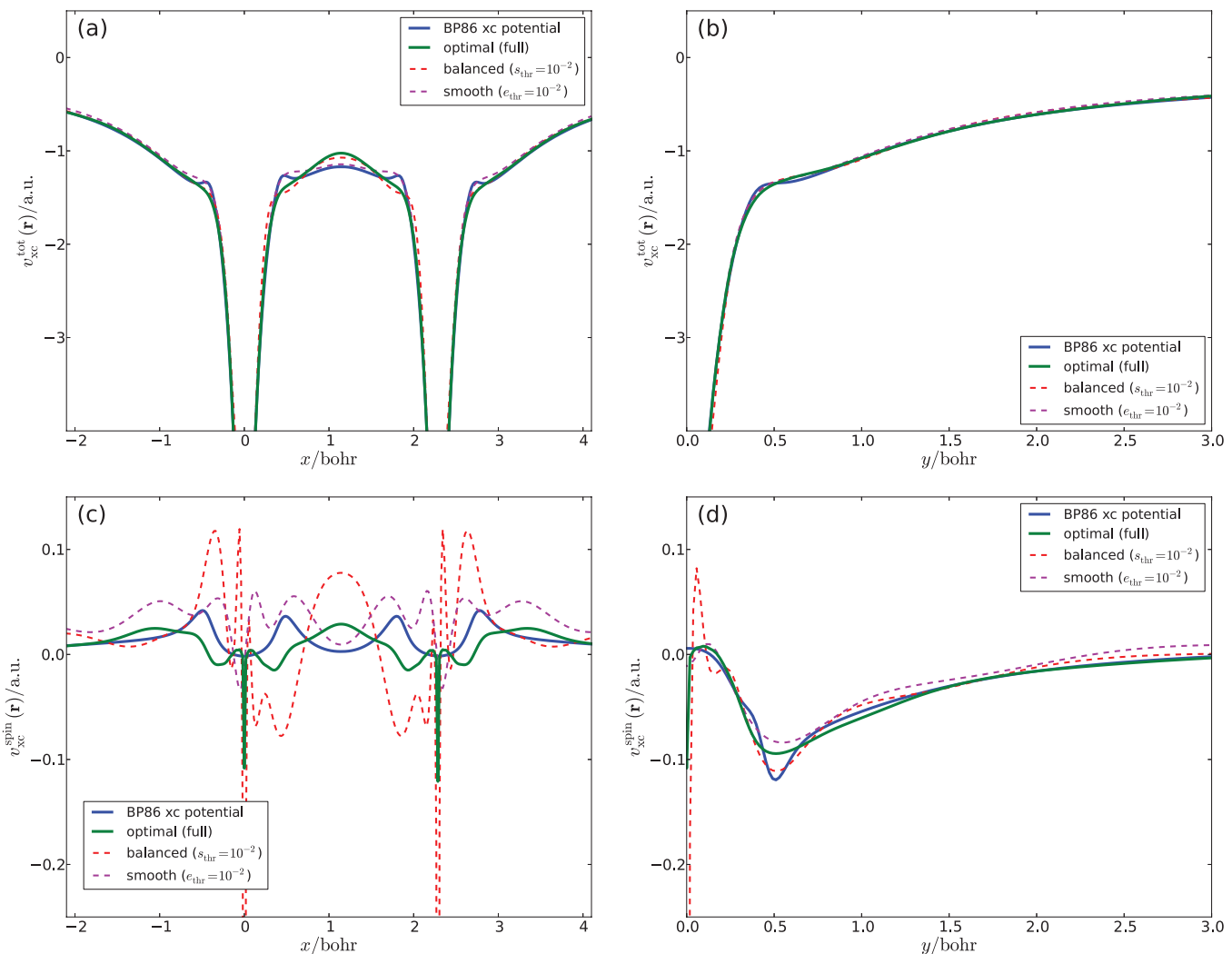


FIG. 5. Reconstructed potentials determined for the dioxygen molecule and a BP86/QZ4P target (spin) density. The upper part shows the total xc potential  $v_{xc}^{\text{tot}}$  (a) along the bond axis ( $x$  axis) and (b) perpendicular to the bond axis along the  $y$  axis. The lower part shows the spin xc potential  $v_{xc}^{\text{spin}}$  along the (c)  $x$  axis and (d)  $y$  axis. In the potential reconstruction, the finite QZ4P orbital basis set was employed. For comparison, the BP86 xc potential calculated from the reference density (“BP86 xc potential”) is also included. This BP86 potential is shifted such that it agrees with the optimal potential at  $x = -2$  bohrs or at  $y = +2$  bohrs, respectively. The corresponding plots of the individual  $\alpha$ - and  $\beta$ -electron potentials are shown in Fig. 8 in the supplementary material.<sup>73</sup>

there is a region where the spin density becomes negative (see the yellow regions in Fig. 4(c)).

The total xc potentials reconstructed for the dioxygen molecule from the BP86/QZ4P target density are shown in Figs. 5(a) and 5(b). For comparison, the figures include the BP86 xc potentials calculated from the target densities. Note, however, that these BP86 potentials are not equal to the exact potentials corresponding to the target densities.<sup>33,48</sup> Therefore, the BP86 potentials should not be reproduced exactly by the potentials reconstructed using a finite orbital basis set.

The different reconstructed total xc potentials all agree rather accurately with the BP86 potential on the scale of the plots. Recognizable differences are only observed along the bond axis in the region between the oxygen atoms. The BP86 potential shows a plateau in this bond region, which is also reproduced by the smooth potential. On the other hand, the balanced as well as the optimal potential do not exhibit such a plateau, but have a maximum at the midbond point. Similar observations can be made for the individual

$\alpha$ - and  $\beta$ -electron potentials (see Fig. 8 in the supplementary material<sup>73</sup>).

The absolute errors  $\Delta_{\text{abs}}^{\sigma, \text{finite}}$  in the  $\alpha$ - and  $\beta$ -electron densities obtained from the different reconstructed potentials within the finite orbital basis set are listed in Table III. Since the QZ4P orbital basis set used for representing the target density is also employed in the potential reconstruction, the WY optimization can be converged such that the error in the  $\alpha$ - and  $\beta$ -electron densities is below  $2.0 \times 10^{-4}$  e bohr $^{-3}$ . This error increases by one order of magnitude for the balanced potential and further increases when determining the optimized potential that is as smooth as possible. Note that these errors depend on the choice of the threshold for discarding small singular values  $s_{\text{thr}}$  and for the change in the density  $e_{\text{thr}}$ , respectively. For the optimal potential, the finite-basis set absolute density error increases further to about  $2 \times 10^{-2}$  e bohr $^{-3}$ . The differences between the reconstructed total and the spin densities and the respective target (spin) density is illustrated in Fig. 15 in the supplementary material.<sup>73</sup> This comparison shows that except for the region close to the nuclei, all reconstructed

TABLE III. Absolute errors  $\Delta_{\text{abs}}^{\alpha,\text{finite}}$  in the  $\alpha$ - and  $\beta$ -electron densities in the finite orbital basis set with respect to the target  $\alpha$ - and  $\beta$ -electron densities (in e bohr $^{-3}$ ) obtained with different reconstructed potentials for the dioxygen molecule. Results are shown for both the target densities from BP86 and from a CAS(12,12)SCF calculation and in the latter case using both the TZ2P and with the QZ4P orbital basis set in the potential reconstruction.

	BP86/QZ4P		CASSCF/TZ2P		CASSCF/QZ4P	
	$\Delta_{\text{abs}}^{\alpha,\text{finite}}$	$\Delta_{\text{abs}}^{\beta,\text{finite}}$	$\Delta_{\text{abs}}^{\alpha,\text{finite}}$	$\Delta_{\text{abs}}^{\beta,\text{finite}}$	$\Delta_{\text{abs}}^{\alpha,\text{finite}}$	$\Delta_{\text{abs}}^{\beta,\text{finite}}$
Wu-Yang	0.0002	0.0002	0.0419	0.0439	0.0412	0.0268
Balanced ( $s_{\text{thr}} = 10^{-2}$ )	0.0019	0.0010	0.0521	0.0537	0.0414	0.0278
Smooth ( $e_{\text{thr}} = 10^{-2}$ )	0.0077	0.0078	0.0426	0.0462	0.0416	0.0277
Optimal (full)	0.0284	0.0230	0.0976	0.0830	0.0640	0.0509

potentials reproduce all qualitative features of the target spin density.

However, to judge the quality of the different potentials, it would be necessary to determine the absolute errors in the  $\alpha$ - and  $\beta$ -electron densities obtained from these potentials in a numerical solution of the KS equations. Unfortunately, this is not easily possible for the molecular system considered here. Nevertheless, for the lithium atom considered above and the atomic systems investigated in Ref. 48, it was demonstrated that this error is the smallest for the optimal potential. Thus, we expect that also for the dioxygen molecule, the optimal potential should be closest to the exact potential.

Finally, we turn to the reconstructed spin xc potentials, which are presented in Figs. 5(c) and 5(d). In the plots along the bond axis (see Fig. 5(c)), both the smooth and the balanced spin potentials deviate significantly from the BP86 spin potential. In particular, the latter shows rather pronounced oscillations. These oscillations were not visible in the plots of the individual  $\alpha$ - and  $\beta$ -electron potentials, but they are amplified when considering the spin potential. The optimal spin potential plotted along the bond axis shows a more regular form and no oscillations that would appear unphysical, but it also differs from the BP86 spin potential. Nevertheless, except for the spikes at the nuclei themselves, it has a similar overall shape near the nuclei, i.e., a symmetric well in which the potential is smaller at the nucleus than ca. 0.5 bohr away from it. This shape of the spin potential corresponds to the positive spin density close to the nuclei. However, in the midbond region, the shape of the optimal spin potential qualitatively differs from the BP86 spin potential and the optimal spin potential shows a maximum at the midbond point, whereas the BP86 spin potential has a minimum. Here, the maximum of the optimal spin potential is actually in line with the nega-

tive spin density at the midbond point. Despite the observed differences, it appears that of the different reconstructed spin potentials, the optimal potential is closest to the BP86 spin potential. Here, it is important to recall that the singly occupied orbitals have a node at the bond axis, i.e., the spin potential here is only responsible for the rather small difference between the doubly occupied  $\alpha$ - and  $\beta$ -electron orbitals (see Fig. 4(a)) and, therefore, it should be relatively small itself.

When inspecting the reconstructed spin potentials perpendicular to the bond axis (see Fig. 5(d)), all reconstructed spin potentials qualitatively agree with the BP86 spin potential. Here, the spin potential is significantly larger than along the bond axis, as it now covers the region to which the singly occupied orbitals extend (cf. Fig. 4(b)). While the differences are small, the optimal spin potential is closest to the BP86 spin potential and only differs at the nucleus, whereas both the smooth and the balanced spin potentials show some oscillatory behavior. The overall shape of the optimal and the BP86 spin potentials in the  $xy$ -plane is compared in Fig. 6. Except for the differences along the bond axis already discussed above, we observe a good overall agreement. With the results obtained for the lithium atom in mind, we attribute these differences to the fact that the BP86 potential does not agree with the exact spin potential, and expect that the optimal spin potential is actually a closer approximation to the exact spin potential.

## 2. CASSCF (spin) density expanded in GTOs

After considering the reconstruction of the spin xc potential for the dioxygen molecule for a BP86/QZ4P target (spin) density, we now turn to an accurate target (spin) density obtained from a CAS(12,12)SCF/cc-pVTZ calculation. This *ab*

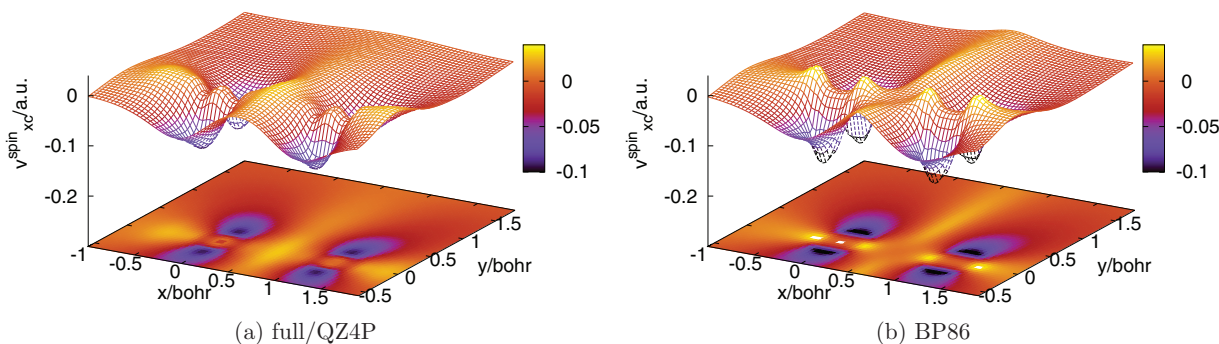


FIG. 6. (a) Reconstructed spin xc potential  $v_{\text{xc}}^{\text{spin}}$  determined for the dioxygen molecule and a BP86/QZ4P target (spin) density in the  $xy$ -plane. Here, only the optimal potential reconstructed within a QZ4P orbital basis set is included. For comparison, (b) shows the BP86 xc potential calculated from the target density.

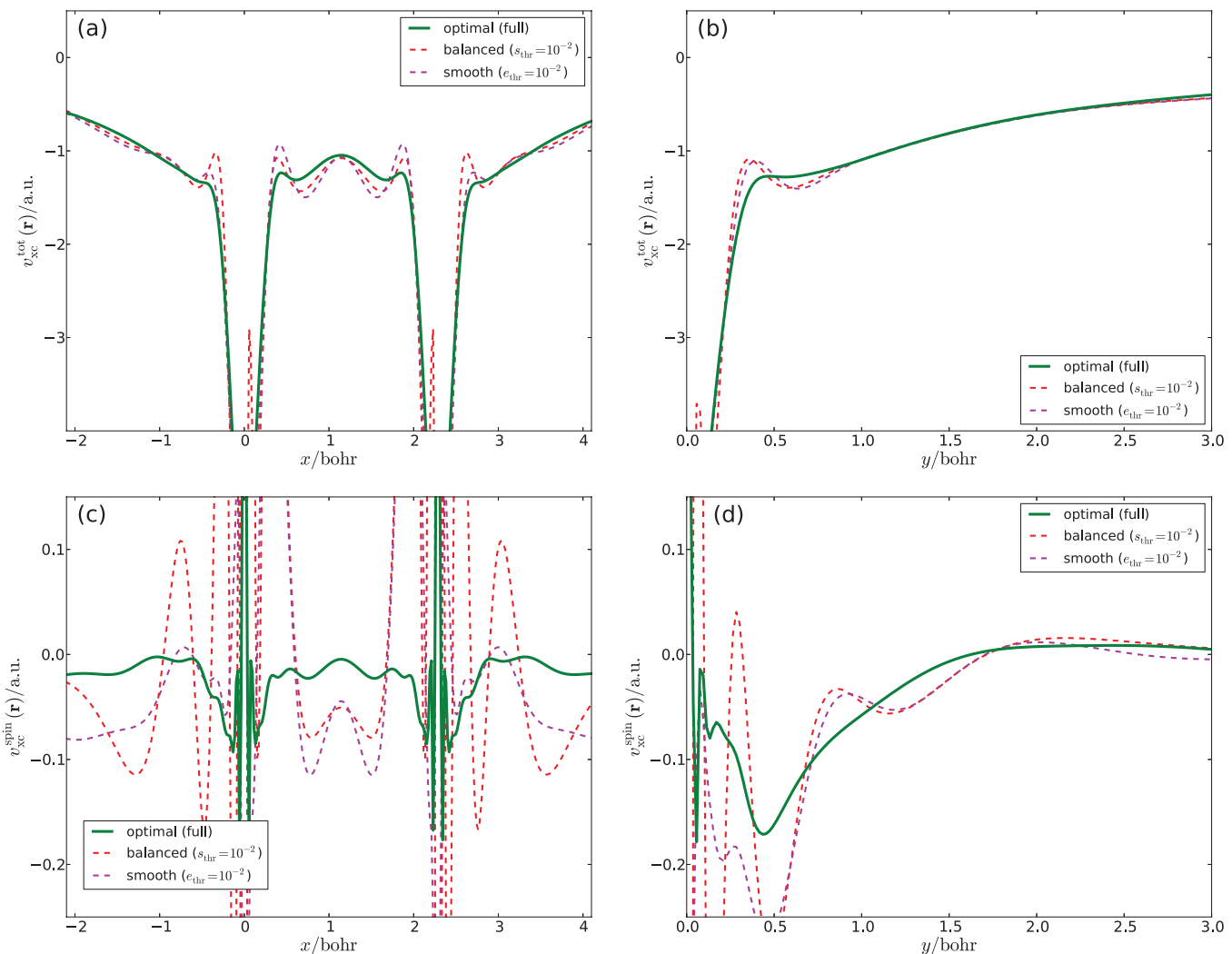


FIG. 7. Reconstructed potentials determined for the dioxygen molecule and a CAS(12,12)SCF/cc-pVTZ target (spin) density. The upper part shows the total xc potential  $v_{xc}^{\text{tot}}$  (a) along the bond axis ( $x$  axis) and (b) perpendicular to the bond axis along the  $y$  axis. The lower part shows the spin xc potential  $v_{xc}^{\text{spin}}$  along the (c)  $x$  axis and (d)  $y$  axis. In the potential reconstruction, the finite QZ4P orbital basis set was employed. The corresponding plots of the individual  $\alpha$ - and  $\beta$ -electron potentials as well as the results obtained with the TZ2P orbital basis set are shown in Figs. 9, 11, and 12 in the supplementary material,<sup>73</sup> respectively.

*initio* spin density is compared to the BP86 spin density in Fig. 4. Perpendicular to the bond axis (see Fig. 4(b)), where the spin density is dominated by the unpaired  $\pi^*$ -electrons, it qualitatively agrees with the one obtained with BP86. Larger differences are found along the bond axis (see Fig. 4(a)), where the spin density is solely due to the difference between the doubly occupied  $\alpha$ - and  $\beta$ -electron orbitals. The CASSCF spin density is significantly larger close to the nuclei, whereas the negative spin density at the ends of the molecule is reduced (see also Fig. 4(d)).

While for the BP86/QZ4P target density the BP86 (spin) potential calculated from the target density could be used for comparison—even though it is not identical to the exact (spin) potential—we now have no reference potential available. Nevertheless, we can still use the results obtained above to judge whether the reconstructed potentials are physically reasonable. The reconstructed total and spin xc potentials obtained using a QZ4P orbital basis set are presented in Fig. 7.

For the reconstructed total xc potential, the optimal potential has a similar shape as the BP86 potential discussed

above. Along the bond axis (see Fig. 7(a)), it has a maximum at the midbond point and exhibits some shell structure at ca. 0.5 bohr from the two nuclei. A similar shape as in the outer region along the bond axis is found perpendicular to the bond axis for the optimal potential (see Fig. 7). Both the smooth and the balanced total potentials have a similar shape, but the shell structure is more pronounced. For the balanced total potential, larger oscillations appear close to the nuclei. Nevertheless, the different reconstructed potentials are qualitatively rather similar. Note that with the smaller TZ2P orbital basis set, larger oscillations appear for the smooth and balanced potentials, whereas the optimal potential is on the scale of the figures in good agreement with the one reconstructed using the larger QZ4P orbital basis set (see Fig. 12 in the supplementary material<sup>73</sup>).

The absolute errors in the reconstructed  $\alpha$ - and  $\beta$ -electron densities in the finite TZ2P and QZ4P orbital basis sets are listed in Table III. Because we are now trying to reproduce target densities expanded in a GTO basis set with STOs, these errors are approximately two orders of magnitude larger

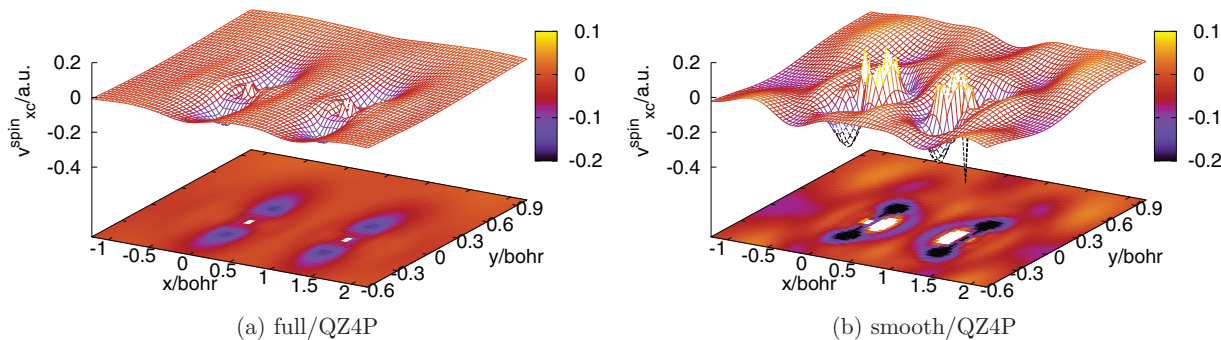


FIG. 8. Reconstructed spin  $xc$  potential potentials determined for the dioxygen molecule and a CAS(12,12)SCF/cc-pVTZ target (spin) density. For the potential reconstruction with the finite QZ4P orbital basis set (a) the optimal spin potential and (b) the spin potential determined by requiring that the optimized potential is smooth are shown. The spin potential obtained by implicitly balancing the orbital and potential basis sets as well as the results obtained with the TZ2P orbital basis set are shown in Fig. 10 and Figs 13 and 14 in the supplementary material,<sup>73</sup> respectively.

than for the STO target densities. The largest finite-basis density errors are found for the optimal potentials. However, we stress again that for judging the quality of the different potentials, it would be necessary to calculate the errors in the densities obtained with a numerical solution of the Kohn-Sham equations on the respective potentials. For the optimal potentials, these numerical density errors, which differ from the finite basis set density errors, should be minimized. With increasing size of the orbital basis set used in the potential reconstruction, the difference between the finite basis set and the numerical density errors should become smaller. Thus, the decrease of the finite basis set density errors when going from TZ2P to QZ4P supports our assumption that the optimal potentials should be closest to the exact potentials (see also Fig. 16 in the supplementary material<sup>73</sup> for a comparison of the difference densities). Furthermore, we note that for both the TZ2P and QZ4P orbital basis sets, the reconstructed potentials are converged with respect to the size of the potential basis set, as is demonstrated in Figs. 17–20 in the supplementary material.<sup>73</sup>

Finally, we now consider the spin  $xc$  potential. Perpendicular to the bond axis (see Fig. 7(d)), the optimal spin potential has a similar shape as the one obtained for the BP86/QZ4P target density with a minimum at ca. 0.5 bohr from the oxygen nuclei, i.e., where the spin density is the largest. In contrast, rather pronounced oscillations are observed for the smooth and balanced spin potentials. These are also present in the plot along the bond axis (see Fig. 7(c)), whereas the optimal potential is mostly well behaved. Qualitatively, it also resembles the optimal spin potential reconstructed from the BP86/QZ4P target density. Around the nuclei, it has negative wells, which are deeper for the CASSCF than for the BP86/QZ4P target density. This is in line with the larger spin density in this region obtained in the CASSCF calculations. In the bond region between the atoms, the optimal spin potential reconstructed from the CASSCF spin density is flatter than in the case of the BP86/QZ4P target density, which agrees with the smaller spin polarization in this region. Very close to the nuclei the reconstructed spin potential has some large oscillations. Most likely, these can be attributed to the deficiencies of the GTO target density, which can cause such oscillations in the exact potentials.<sup>84</sup>

To compare the overall performance of the different potential reconstruction schemes, Fig. 8 compares the optimal and the smooth spin potentials in the  $xy$ -plane. A similar comparison for the balanced spin potential is shown in Fig. 10 in the supplementary material.<sup>73</sup> While pronounced wiggling features around the position of the nuclei are found in the smooth spin potential, it is obvious that these can be eliminated in the whole  $xy$ -plane for the optimal spin potential. Thus, even though there is no exact reference spin potential available for comparison, we find that the optimal spin potential is the only one that seems to be free of artifacts of the potential reconstruction. Moreover, the comparison with the spin potential reconstructed from the BP86/QZ4P target density shows that the optimal potential is physically reasonable. Therefore, we are confident that it is the reconstructed potential that is closest to the exact spin potential.

Further support for this conclusion can be drawn from a comparison with the reconstructed potentials obtained for the same CASSCF target density with the smaller TZ2P orbital basis set, which are shown in Figs. 11, 13, and 14 in the supplementary material.<sup>73</sup> Here, even larger oscillations are found for the smooth and balanced spin potentials, even though the same thresholds are applied. On the other hand, the optimal potentials are qualitatively similar to the QZ4P results. This is particularly obvious for the spin potential perpendicular to the bond axis, which is in good agreement with the one reconstructed with the QZ4P orbital basis set. Also along the bond axis the shapes of the optimal spin potentials are similar for the two orbital basis sets, even though the negative well near the oxygen nuclei is less pronounced. Thus, only for the optimal potential a consistent convergence with increasing size of the orbital basis set is observed.

## V. CONCLUSIONS

In this work, we have extended the unambiguous reconstruction of the local potential yielding a given target density<sup>48</sup> to open-shell systems treated with an unrestricted KS-DFT formalism. Moreover, we have combined this reconstruction with the use of accurate target (spin) densities obtained from accurate wave-function based *ab initio* calculations, i.e., from Full-CI or CASSCF wave functions. This

provides a route to accurate reference data for the spin xc potential  $v_{xc}^{\text{spin}}$ , which determines the spin density distribution  $Q(\mathbf{r})$  in unrestricted KS-DFT.

Reconstructing this spin xc potential is a particularly challenging task, because it is given by the difference between the reconstructed  $\alpha$ - and  $\beta$ -electron potentials. Thus, one has to overcome the numerical inaccuracies caused by the ill-posed nature of the potential reconstruction problem in finite orbital basis sets, as these could otherwise be amplified when calculating the spin potential. As test cases, we chose the lithium atom and the oxygen molecule in its triplet state. For both systems, we considered target (spin) densities from unrestricted KS-DFT calculations as well as from Full-CI (for the lithium atom) and CASSCF (for the dioxygen molecule) calculations. These test cases made it possible to systematically assess the quality of the reconstructed spin xc potentials.

For the lithium atom, it is possible to compare the reconstructed potentials to the exact ones, which can be obtained from a fully numerical potential reconstruction. The comparison shows that the optimal spin potentials, determined using the scheme of Ref. 48, can reproduce the fully numerical spin potential, while the spin potentials obtained by singling out the  $\alpha$ - and  $\beta$ -electron potentials that are as smooth as possible or with an implicitly balanced potential basis set show significantly larger deviations from the reference spin potential. In general, the quality of these smooth and balanced spin potentials strongly depends on the choice of the corresponding threshold values and can result in highly oscillating potentials if these are chosen too small. On the other hand, if these thresholds are too large, the resulting potentials lack all features present in the exact one. Moreover, different thresholds might be required for reconstructing the  $\alpha$ - and  $\beta$ -electron potentials in order to obtain these with similar quality, as is required for the reconstruction of the spin potential. Thus, we conclude that the unambiguous potential reconstruction method of Ref. 48 should be used if accurate spin potentials are sought.

For target densities obtained with GTO orbital basis sets, which are commonly used in wave-function based *ab initio* calculations, we found it advantageous to reconstruct the potential using a STO orbital basis set. In this case, the density obtained from the WY optimization, which is the first step in all potential reconstruction schemes tested here, has the correct shape close to the nuclei and in the asymptotic region. Consequently, oscillations close to the nucleus found in the fully numerical reference potential because of the wrong form of the GTO target density<sup>84</sup> are largely suppressed in the optimal reconstructed potentials. When using a GTO orbital basis sets in combination with the scheme of Ref. 48, these oscillations might result in artifacts in the reconstructed potentials. On the other hand, the use of a STO orbital basis set requires the use of a basis set that is large enough to reproduce the *ab initio* target (spin) density. Here, we found that the a QZ4P orbital basis set is sufficient to obtain a good agreement with the target density. Moreover, we note that technical improvements to our implementation, in particular, the use of a Tikhonov regularization in the WY optimization<sup>74</sup> and the use of a cut-off value for discarding small density regions in the criterion of Eq. (20), were necessary to treat GTO target densities.

For the dioxygen molecule, a direct comparison to a fully numerical reference spin potential is not possible. Nevertheless, for the target density obtained from an unrestricted KS-DFT calculation the xc potential used for determining the target potential can provide some guidance, even though it differs from the exact potential because of the use of a finite orbital basis set. This comparison shows that the optimal reconstructed spin potential (i.e., the one obtained using the scheme of Ref. 48) shows the best overall agreement. Also for the CASSCF target density, this scheme is the only one that provides a physically reasonable spin xc potential, while the smooth and the balanced potentials are plagued by unphysical oscillations. The optimal potential shows such oscillations only very close to the nuclei, where they are probably due to deficiencies of the GTO expansion used for the target density.

In summary, we believe that the potential reconstruction scheme proposed in Ref. 48 and extended here to open-shell systems provides the first reliable approach for reconstructing the spin xc potential from accurate *ab initio* (spin) densities. The availability of such accurate reference spin potentials can facilitate the development of improved spin-dependent xc density functionals which apart from yielding accurate total electron densities also provide reliable spin densities. Thus, this work represents a prerequisite for the design of approximate xc functional with an improved spin-density dependence.

## ACKNOWLEDGMENTS

M.R. and K.B. gratefully acknowledge financial support by a grant from the Swiss National Science Foundation (SNF). K.B. thanks the Fonds der Chemischen Industrie for a Chemiefonds scholarship. C.R.J. acknowledges funding from the DFG-Center for Functional Nanostructures (CFN) at KIT.

- <sup>1</sup>R. G. Parr and W. Yang, *Density-Functional Theory of Atoms and Molecules* (Oxford University Press, 1989).
- <sup>2</sup>E. Engel and R. M. Dreizler, *Density Functional Theory: An Advanced Course*, 1st ed. (Springer, Berlin, 2011).
- <sup>3</sup>W. Koch and M. Holthausen, *A Chemist's Guide to Density Functional Theory* (Wiley, 2001).
- <sup>4</sup>C. J. Cramer and D. G. Truhlar, *Phys. Chem. Chem. Phys.* **11**, 10757 (2009).
- <sup>5</sup>M. Reiher, *Faraday Discuss.* **135**, 97 (2007).
- <sup>6</sup>M. Reiher, *Chimia* **63**, 140 (2009).
- <sup>7</sup>M. Reiher, O. Salomon, and B. A. Hess, *Theor. Chem. Acc.* **107**, 48 (2001).
- <sup>8</sup>M. Reiher, *Inorg. Chem.* **41**, 6928 (2002).
- <sup>9</sup>J. N. Harvey, *Struct. Bonding* **112**, 151 (2004).
- <sup>10</sup>S. Ye and F. Neese, *Inorg. Chem.* **49**, 772 (2010).
- <sup>11</sup>M. Swart, *Int. J. Quantum Chem.* **113**, 2–7 (2013).
- <sup>12</sup>A. Ghosh, *J. Biol. Inorg. Chem.* **11**, 712 (2006).
- <sup>13</sup>J. Conradie and A. Ghosh, *J. Phys. Chem. B* **111**, 12621 (2007).
- <sup>14</sup>M. Radon and K. Pierloot, *J. Phys. Chem. A* **112**, 11824 (2008).
- <sup>15</sup>K. Boguslawski, Ch. R. Jacob, and M. Reiher, *J. Chem. Theory Comput.* **7**, 2740 (2011).
- <sup>16</sup>R. van Leeuwen and E. J. Baerends, *Phys. Rev. A* **49**, 2421 (1994).
- <sup>17</sup>O. Gritsenko, P. Schipper, and E. Baerends, *Chem. Phys. Lett.* **302**, 199 (1999).
- <sup>18</sup>T. W. Keal and D. J. Tozer, *J. Chem. Phys.* **119**, 3015 (2003).
- <sup>19</sup>T. W. Keal and D. J. Tozer, *J. Chem. Phys.* **121**, 5654 (2004).
- <sup>20</sup>M. J. G. Peach, A. M. Teale, and D. J. Tozer, *J. Chem. Phys.* **126**, 244104 (2007).
- <sup>21</sup>A. M. Teale, S. Coriani, and T. Helgaker, *J. Chem. Phys.* **132**, 164115 (2010).
- <sup>22</sup>P. D. Elkind and V. N. Staroverov, *J. Chem. Phys.* **136**, 124115 (2012).

- <sup>23</sup>J. Karwowski, *Int. J. Quantum Chem.* **109**, 2456 (2009).
- <sup>24</sup>A. S. P. Gomes and Ch. R. Jacob, *Annu. Rep. Prog. Chem., Sect. C: Phys. Chem.* **108**, 222 (2012).
- <sup>25</sup>O. Roncero, M. P. de Lara-Castells, P. Villarreal, F. Flores, J. Ortega, M. Paniagua, and A. Aguado, *J. Chem. Phys.* **129**, 184104 (2008).
- <sup>26</sup>O. Roncero, A. Zanchet, P. Villarreal, and A. Aguado, *J. Chem. Phys.* **131**, 234110 (2009).
- <sup>27</sup>J. Nafziger, Q. Wu, and A. Wasserman, *J. Chem. Phys.* **135**, 234101 (2011).
- <sup>28</sup>J. D. Goodpaster, T. A. Barnes, and T. F. Miller III, *J. Chem. Phys.* **134**, 164108 (2011).
- <sup>29</sup>C. Huang, M. Pavone, and E. A. Carter, *J. Chem. Phys.* **134**, 154110 (2011).
- <sup>30</sup>J. D. Goodpaster, T. A. Barnes, F. R. Manby, and T. F. Miller, *J. Chem. Phys.* **137**, 224113 (2012).
- <sup>31</sup>S. Fux, Ch. R. Jacob, J. Neugebauer, L. Visscher, and M. Reiher, *J. Chem. Phys.* **132**, 164101 (2010).
- <sup>32</sup>J. D. Goodpaster, N. Ananth, F. R. Manby, and T. F. Miller III, *J. Chem. Phys.* **133**, 084103 (2010).
- <sup>33</sup>P. de Silva and T. A. Wesolowski, *J. Chem. Phys.* **137**, 094110 (2012).
- <sup>34</sup>S. Liu and P. W. Ayers, *Phys. Rev. A* **70**, 022501 (2004).
- <sup>35</sup>Ch. R. Jacob, S. M. Beyhan, and L. Visscher, *J. Chem. Phys.* **126**, 234116 (2007).
- <sup>36</sup>J. D. Talman and W. F. Shadwick, *Phys. Rev. A* **14**, 36 (1976).
- <sup>37</sup>A. Görling, *Phys. Rev. A* **46**, 3753 (1992).
- <sup>38</sup>W. Yang and Q. Wu, *Phys. Rev. Lett.* **89**, 143002 (2002).
- <sup>39</sup>Q. Wu and W. Yang, *J. Chem. Phys.* **118**, 2498 (2003).
- <sup>40</sup>E. Engel and R. M. Dreizler, *J. Comput. Chem.* **20**, 31 (1999).
- <sup>41</sup>A. Makmal, S. Kümmel, and L. Kronik, *J. Chem. Theory Comput.* **5**, 1731 (2009).
- <sup>42</sup>V. N. Staroverov, G. E. Scuseria, and E. R. Davidson, *J. Chem. Phys.* **124**, 141103 (2006).
- <sup>43</sup>T. Heaton-Burgess, F. Bulat, and W. Yang, *Phys. Rev. Lett.* **98**, 256401 (2007).
- <sup>44</sup>A. Heßelmann, A. W. Götz, F. Della Sala, and A. Görling, *J. Chem. Phys.* **127**, 054102 (2007).
- <sup>45</sup>C. Kollmar and M. Filatov, *J. Chem. Phys.* **127**, 114104 (2007).
- <sup>46</sup>J. Fernandez, C. Kollmar, and M. Filatov, *Phys. Rev. A* **82**, 022508 (2010).
- <sup>47</sup>F. Bulat, T. Heaton-Burgess, A. J. Cohen, and W. Yang, *J. Chem. Phys.* **127**, 174101 (2007).
- <sup>48</sup>Ch. R. Jacob, *J. Chem. Phys.* **135**, 244102 (2011).
- <sup>49</sup>O. V. Gritsenko and E. J. Baerends, *J. Chem. Phys.* **120**, 8364 (2004).
- <sup>50</sup>U. von Barth and L. Hedin, *J. Phys. C* **5**, 1629 (1972).
- <sup>51</sup>Ch. R. Jacob and M. Reiher, *Int. J. Quantum Chem.* **112**, 3661 (2012).
- <sup>52</sup>M. Kaupp, M. Bühl, and V. G. Malkin, *Calculation of NMR and EPR Parameters. Theory and Applications* (Wiley-VCH, Weinheim, 2004).
- <sup>53</sup>R. McWeeny and B. T. Sutcliffe, *Methods of Molecular Quantum Mechanics* (Academic, New York, 1969).
- <sup>54</sup>R. McWeeny, *Spin in Chemistry* (Dover, New York, 2004).
- <sup>55</sup>E. R. Davidson, *Reduced Density Matrices in Quantum Chemistry* (Academic, New York, 1976).
- <sup>56</sup>J. A. Pople, P. M. W. Gill, and N. C. Handy, *Int. J. Quantum Chem.* **56**, 303 (1995).
- <sup>57</sup>J. P. Perdew, A. Ruzsinszky, L. A. Constantin, J. Sun, and G. I. Csonka, *J. Chem. Theory Comput.* **5**, 902 (2009).
- <sup>58</sup>A. J. Cohen, P. Mori-Sánchez, and W. Yang, *J. Chem. Phys.* **129**, 121104 (2008).
- <sup>59</sup>A. J. Cohen, P. Mori-Sánchez, and W. Yang, *Chem. Rev.* **112**, 289 (2012).
- <sup>60</sup>Y. Wang and R. G. Parr, *Phys. Rev. A* **47**, R1591 (1993).
- <sup>61</sup>Q. Zhao, R. C. Morrison, and R. G. Parr, *Phys. Rev. A* **50**, 2138 (1994).
- <sup>62</sup>F. Colonna and A. Savin, *J. Chem. Phys.* **110**, 2828 (1999).
- <sup>63</sup>E. S. Kadantsev and M. J. Stott, *Phys. Rev. A* **69**, 012502 (2004).
- <sup>64</sup>O. V. Gritsenko, R. van Leeuwen, and E. J. Baerends, *Phys. Rev. A* **52**, 1870 (1995).
- <sup>65</sup>P. R. T. Schipper, O. V. Gritsenko, and E. J. Baerends, *Theor. Chem. Acc.* **99**, 329 (1998).
- <sup>66</sup>S. Hirata, S. Ivanov, I. Grabowski, R. J. Bartlett, K. Burke, and J. D. Talmann, *J. Chem. Phys.* **115**, 1635 (2001).
- <sup>67</sup>G. L. Oliver and J. P. Perdew, *Phys. Rev. A* **20**, 397 (1979).
- <sup>68</sup>M. Levy, *Proc. Natl. Acad. Sci. U.S.A.* **76**, 6062 (1979).
- <sup>69</sup>M. Levy, *Phys. Rev. A* **26**, 1200 (1982).
- <sup>70</sup>T. Heaton-Burgess and W. Yang, *J. Chem. Phys.* **129**, 194102 (2008).
- <sup>71</sup>G. te Velde, F. M. Bickelhaupt, E. J. Baerends, C. Fonseca Guerra, S. J. A. van Gisbergen, J. G. Snijders, and T. Ziegler, *J. Comput. Chem.* **22**, 931 (2001).
- <sup>72</sup>Ch. R. Jacob, S. M. Beyhan, R. E. Bulo, A. S. P. Gomes, A. W. Götz, K. Kiewisch, J. Sikkema, and L. Visscher, *J. Comput. Chem.* **32**, 2328 (2011).
- <sup>73</sup>See supplementary material at <http://dx.doi.org/10.1063/1.4788913> for further numerical studies on the reconstruction procedure.
- <sup>74</sup>Q. Wu and W. Yang, *J. Theor. Comput. Chem.* **2**, 627 (2003).
- <sup>75</sup>A. N. Tihonov, *Dokl. Akad. Nauk SSSR* **151**, 501 (1963).
- <sup>76</sup>W. H. Press, A. A. Teukolsky, W. T. Vetterling, and B. P. Flannery, *Numerical Receipes: The Art of Scientific Computing*, 3rd ed. (Cambridge University Press, 2007).
- <sup>77</sup>M. J. G. Peach, D. G. J. Griffiths, and D. J. Tozer, *J. Chem. Phys.* **136**, 144101 (2012).
- <sup>78</sup>P. de Silva and T. A. Wesolowski, *Phys. Rev. A* **85**, 032518 (2012).
- <sup>79</sup>D. Andrae and J. Hinze, *Int. J. Quantum Chem.* **63**, 65 (1997).
- <sup>80</sup>G. Eickerling and M. Reiher, *J. Chem. Theory Comput.* **4**, 286 (2008).
- <sup>81</sup>H.-J. Werner, P. J. Knowles, R. Lindh, F. R. Manby, M. Schütz *et al.*, MOLPRO, version 2009.1, a package of *ab initio* programs, 2009, see <http://www.molpro.net>.
- <sup>82</sup>T. H. Dunning, Jr., *J. Chem. Phys.* **90**, 1007 (1989).
- <sup>83</sup>N. B. Balabanov and K. A. Peterson, *J. Chem. Phys.* **123**, 064107 (2005).
- <sup>84</sup>P. R. T. Schipper, O. V. Gritsenko, and E. J. Baerends, *Theor. Chem. Acc.* **98**, 16 (1997).